FIELD INSTRUMENTATION AND TESTING OF HIGH-MAST LIGHTING TOWERS IN THE STATE OF IOWA

DRAFT FINAL REPORT

January 2006

Prepared for:

Iowa Department of Transportation
Office of Bridges and Structures
800 Lincoln Way
Ames, IA 50010

Technical Contact:
Bruce Brakke
Phone: (515) 239-1165
Fax: (515) 239-1978
Email: Bruce.Brakke@dot.state.ia.us

Prepared by:

Robert J. Connor, Ph.D **Ian C. Hodgson, P.E., S.E.**

Table of Contents

Acknowledgements

The authors would like to acknowledge the efforts of the research team from Iowa State University in Ames, Iowa, namely, Terry Wipf, Brent Phares, Nick Burdine, Doug Wood, and Byung-Ik Chang. The Iowa State team was responsible for installing and maintaining the data acquisition system at the Clear Lake site for the duration of the monitoring.

The field instrumentation and testing portion of this project was performed by researchers with the Infrastructure Monitoring Program at Lehigh University's Center for Advanced Technology for Large Structural Systems (ATLSS). The authors were involved in this phase of the project as members of this team. The efforts in the field of Carl Bowman (instrumentation technician) and Margaret Warpinski (graduate student in structural engineering at Lehigh) were critical to the success of the project.

All data interpretation and report preparation were performed by the authors acting as consultants to the Iowa Department of Transportation. All opinions expressed in this report are those of the authors and do not necessarily represent those of Lehigh University.

Executive Summary

As a result of the collapse of a 140 foot high-mast tower in Sioux City, Iowa in November of 2003, a thorough investigation into the behavior and design of these tall, yet relatively flexible structures was undertaken. Extensive work regarding the root cause of this failure was carried out by Robert Dexter of The University of Minnesota. Furthermore, a statewide study of all the high-mast towers in Iowa revealed fatigue cracks and loose anchor bolts on many other existing structures.

The current study was proposed to examine the static and dynamic behavior of a variety of poles in the State of Iowa utilizing field testing, specifically long-term monitoring and load testing. This report presents the results and conclusions from this project.

The field work for this project was divided into two phases. Phase 1 of the project was conducted in October 2004 and focused on the dynamic properties of ten different poles in Clear Lake, Ames, and Des Moines, Iowa. Of those ten, two were also instrumented to obtain stress distributions at various details and were included in a 12 month long-term monitoring study. Phase 2 of this investigation was conducted in May of 2005, in Sioux City, Iowa, and focused on determining the static and dynamic behavior of a pole similar to the one that collapsed in November 2003. Identical tests were performed on a similar pole which was retrofitted with a more substantial replacement bottom section in order to assess the effect of the retrofit. A third pole with different details was dynamically load tested to determine its dynamic characteristics, similar to the Phase 1 testing.

Based on the dynamic load tests, the modal frequencies of the poles fall within the same range. Also, the damping ratios are significantly lower in the higher modes than the values suggested in the AASHTO and CAN/CSA specifications. The comparatively higher damping ratios in the first mode may be due to aerodynamic damping. These low damping ratios in combination with poor fatigue details contribute to the accumulation of a large number of damage-causing cycles.

As predicted, the stresses in the original Sioux City pole are much greater than the stresses in the retrofitted poles at Sioux City. Additionally, it was found that poor installation practices which often lead to loose anchor bolts and out-of-level leveling nuts can cause high localized stresses in the pole, which can accelerate fatigue damage.

1.0 Background

On November 12, 2003, a 140-foot high-mast tower along I-29 in Sioux City, Iowa collapsed. The wind speed at the time of the collapse was reported to be 37 mph, with maximum wind speeds earlier in the day of 56 mph. An extensive study into the root cause of the failure was carried out by the late Robert Dexter of the University of Minnesota and sub-consultants Robert J. Connor, Ian C. Hodgson, and Eric Kaufman. The results are presented in a report prepared for the Iowa DOT in September 2004 [1].

1.1 Prior Studies

The collapse of the tower in Sioux City prompted a statewide investigation of all the high-mast lighting towers in Iowa. Of the 233 towers inspected, 17 galvanized high-mast towers similar to the collapsed tower, and 3 weathering steel high-mast towers near Clear Lake, Iowa were found to have cracks. All of the cracked towers have been taken down. The bottom sections of the towers in Sioux City have been replaced and a "jacket" retrofit has been installed on the towers near Clear Lake. Additionally, loose anchor nuts on top of the baseplates and leveling nuts not in contact with the baseplate were discovered at 32 towers during the investigation. A statewide retightening program was implemented.

1.2 Objectives of the Current Study

The current study was initiated to quantify the stresses induced in the critical components of the towers, characterize the wind phenomena producing fatigue damage in the high mast towers, and to identify and measure the key dynamic properties of a variety of towers to provide for more accurate predictions of tower response. These three objectives were accomplished using field instrumentation, testing, and long-term monitoring of a select number of towers.

The field work for the project was divided into two phases. The first phase focused on a number high-mast towers in the Clear Lake, Ames, and Des Moines areas. The second phase of the field work concerned a number of towers in the Sioux City area. Specifically, the differences in the dynamic and static behavior between a tower very similar to the collapsed tower and a similar but retrofitted tower were studied.

1.3 Summary of the Field Testing Program

1.3.1 Phase 1

Installation of all sensors and load testing for Phase 1 of the field study was conducted during the week of October 11, 2004. During Phase 1, 10 towers were instrumented and tested, as listed in Table 2.1. The towers were located at five interchanges in Clear Lake, Ames, and Des Moines, Iowa. Two towers in each interchange were tested to assess the repeatability of tests preformed on towers with the same design. Towers of varying material (galvanized vs. weathering), geometry (height, material thickness, anchor rod pattern, etc.), and age were tested.

Of the towers tested, two towers in Clear Lake were instrumented with strain gages to obtain stress distributions at various details. The first tower was uncracked and had not be retrofitted prior to testing. In this report, this tower is termed the *"As-built tower."*

The second tower had been retrofitted with a steel splice jacket at the base as seen in Figure 1.1. The retrofit was designed by Wiss, Janney, Elstner, and Associates. Strain gages were installed on both the splice jacket and on the original tower just above the jacket. This tower is termed the *"Retrofit tower."*

Figure 1.1 – Jacket retrofit designed by Wiss, Janney, Elstner, and Associates and installed in Clear Lake, Iowa

Both towers were included in a 12 month long-term monitoring program to obtain information regarding the response of the towers under natural wind loading. During the 12 month monitoring period, ambient vibration data were recorded (for 15 to 30 minutes) when wind speeds exceeded predetermined trigger levels. Furthermore, wind speed and direction were continuously monitored.

In addition to the long-term monitoring program, a series of dynamic loading tests were conducted on all 10 of the towers listed in Table 1.1. These tests were conducted by statically loading the towers with a cable fixed at one end, and connected to the tower approximately 35 feet above the base, as shown in Figure 1.2. The load was subsequently released rapidly to allow the tower to vibrate freely. These dynamic, or "pluck," tests produced a free decay vibration signature that can be used to extract the both the natural frequencies and damping characteristics of the high-mast tower.

County	Tower Location	Tower Number	Material G or W	Tower Height (ft)	Tower Diameter at Base (in)	Number of Sides	Tower Wall Thickness at Base (in)	Base Plate Thickness (in)	Anchor Rod Pattern	Number of Anchor Rods	Comments
Story	I-35/US-30	6	W	100	22	12	-	1.75	S	4	Anchor chairs
		7	W	100	22	12	-	1.75	S	4	Anchor chairs
Polk	I-80/1-35/I-235 NW Interchange	3	W	140	29.5	12	1/2	2.75	C	12	Anchor chairs
		7	W	145	30.1	12	1/2	3.00	C	12	Anchor chairs
Polk	I-80/1-35/I-235 NE Interchange	7	W	140	-	-	-	-	C	6	-
		8	W	140	-	-	-	-	C	6	-
Warren	IA-5 & US65/US69	2	G	120	22	Round	1/4	1.50	C	6	-
		8	G	120	22	Round	1/4	1.50	C	6	-
Cerro Gordo	I-35/US18	1	W	148	28.5	12	5/16	1.75	C	6	As-built Tower
		7	W	148	28.5	12	5/16	1.75	C	6	Retrofit Tower

Notes:
W – Weathering Steel
G – Galvanized
C – Circular
S – Square

Table 1.1 – Summary of all high-mast towers instrumented and tested during Phase 1 of the study

Figure 1.2 – Typical dynamic test of a retrofitted tower along I-29 in Sioux City, Iowa

1.3.2 Phase 2

Phase 2 of the field study was conducted on May 10-11, 2005. During Phase 2, two towers at the interchange between I-29 and US-20 in Sioux City were instrumented and tested to obtain the dynamic characteristics and the magnitude of stresses at critical details. The first tower tested is identical to the tower that collapsed in 2003. The second tower that was tested is a retrofitted tower with a new base section with a revised hand-hole detail, a thicker baseplate, and a 5/8 inch wall thickness (compared to the 3/16 inch thickness of the original tower). The instrumentation plans for the two towers was nearly identical. Furthermore, identical tests were performed at the two towers. Figure 2.2 contains photographs of the original and retrofit towers. The purpose of these tests is to compare static and dynamic behavior of the original and retrofitted towers. A third and different type of tower located at the Hamilton Road exit of I-29, was also instrumented to obtain its dynamic characteristics to add to the range of tower types tested in Phase 1. Only dynamic properties were obtained at this third tower.

2.0 Instrumentation Plan and Data Acquisition

The following sections describe the sensors and instrumentation plan used during the static/dynamic testing and the long-term monitoring programs for Phases 1 and 2 of the field efforts. Detailed instrumentation plans can be found in Appendix A.

2.1 Strain Gages

Strain were placed at predetermined locations. All strain gages installed in the field were produced by Measurements Group Inc. and were 0.25 inch gage length, model LWK-06-W250B-350. These gages are uniaxial weldable resistance-type strain gages. Weldable-type strain gages were selected due to the ease of installation in a variety of weather conditions. The "welds" are point or spot resistance welds about the size of a pin prick. The probe is powered by a battery and only touches the foil that the strain gage is mounted on by the manufacturer. This fuses the foil to the steel surface. It takes forty or more of these small "welds" to attach the gage to the steel surface. There are no arc strikes or heat affected zones that are discernible. There is no preheat or any other preparation involved other than the preparation of the local metal surface by grinding and then cleaning before the gage is attached to the component with the welding unit. There has never been an instance of adverse behavior associated with the use of weldable strain gages including their installation on extremely brittle material such as A615 Gr75 steel reinforcing bars.

These strain gages are also temperature compensated and perform very well when accurate strain measurements are required over long periods of time (months to years). The gage resistance is 350 ohms and an excitation voltage of 10 volts was used. All gages were protected with a multi-layer weatherproofing system and then sealed with a silicon type compound.

2.2 Accelerometers

Uniaxial accelerometers were used in all phases of the study. The As-built tower at the Clear Lake location had four permanent sensors installed for the duration of the long-term monitoring. For all of the pluck tests conducted as part of both Phase 1 and 2, the sensors were temporarily mounted to the test tower using hose clamps.

All of the accelerometers were manufactured by PCB Piezotronics, Inc. models 3701G3FA50G (used for the permanent installation at Clear Lake) and 3701G3FA3G (used for all temporary installations used for the pluck tests). The former has a peak measurable acceleration of 50 g, while for the latter, the peak is 3 g.

These accelerometers are termed capacitive (or DC) accelerometers. The primary component of these sensors is an internal capacitor. When subjected to acceleration, the sensor outputs a voltage in direct proportion to the magnitude of the acceleration. They are specifically designed for measuring low-level, low-frequency accelerations, such as that found on a bridge or a high-mast lighting tower. A photograph of a typical accelerometer used for this project is shown in Figure 2.1. Note that the measurement axis is normal to the top face of the sensor. An example of a temporary mounting using hose clamps is shown in Figure 2.2.

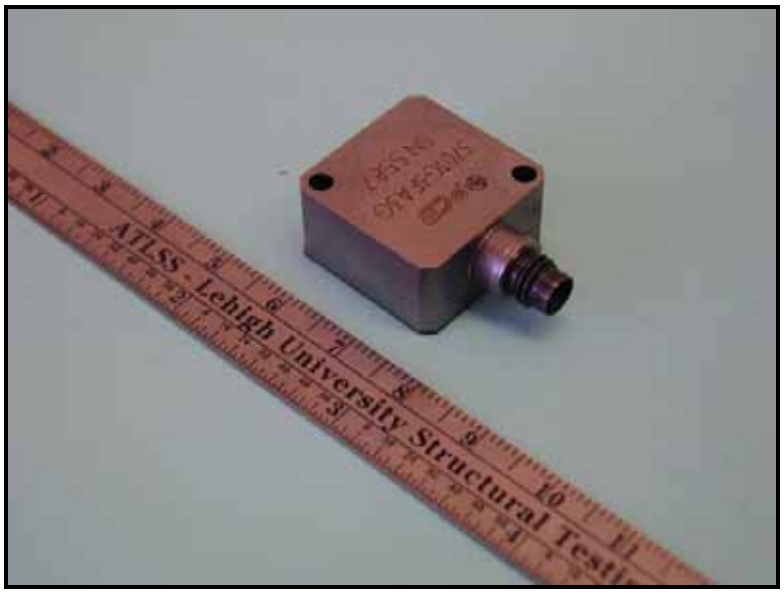

Figure 2.1 – PCB capacitive accelerometer (model 3701G3FA3G shown)

Figure 2.2 – Temporary accelerometer mounting used for the dynamic tests

2.3 Anemometers

An anemometer was used to measure wind speed and direction at the As-built and Retrofit towers during the long-term monitoring phase of the project. At the As-built tower, the anemometer was installed atop a 30 foot wooden telephone pole directly adjacent to the high-mast tower. The anemometer (model number 5103) is manufactured by R.M. Young Inc., and is a propeller type anemometer. Both wind speed and wind direction are measured.

At the Retrofit tower, three anemometers were installed at different heights up the tower, equal to 33 feet, 86 feet 6 inches, and 140 feet above the base plate. Figure 2.3 contains a photograph of the Retrofit tower with the anemometer installed. The anemometers were mounted to the tower with brackets as shown in Figure 2.4. The lowest anemometer is a R.M. Young model 5103 anemometer identical to that at the As-built tower. The upper two anemometers are 3-cup anemometers which only record the wind speed. They are manufactured by R.M. Young Inc., model 3101.

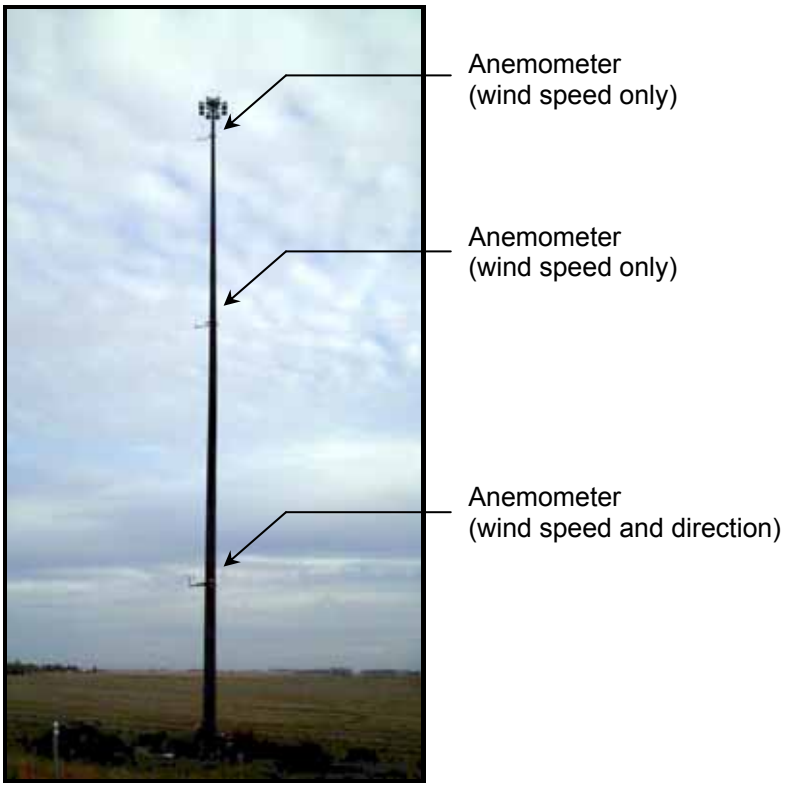

Figure 2.3 – Retrofit tower along US-18 in Clear Lake, IA, with anemometers installed

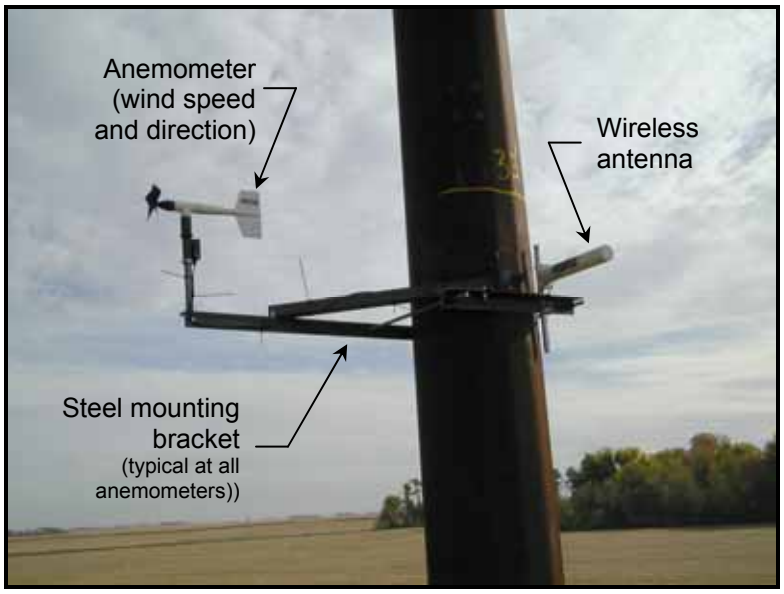

Figure 2.4 – Anemometer installed at 33 feet above the base plate
at Retrofit tower along US-18 in Clear Lake, IA

2.4 Data Acquisition Systems

2.4.1 As-built Tower – Clear Lake

The installation and maintenance of the instrumentation and data acquisition system at the As-built tower was performed by researchers at Iowa State University. A Campbell Scientific CR9000 data logger was used for the collection of data at the As-built tower in Clear Lake during the long-term monitoring phase. This logger is a high speed, multi-channel 16-bit data acquisition system. The data logger was configured with digital and analog filters to assure noise-free signals. Note that during the static and dynamic testing of this tower only, a separate data acquisition system furnished by researchers from Iowa State University was used.

The data logger was enclosed in a weather-tight box adjacent to the tower, as seen in Figure 2.5. Remote communications with the data logger was established using a satellite internet connection (see Figure 2.5). Data collection managed by the Iowa State researchers and was performed automatically via a server located at the Iowa State University. The satellite link was also used to upload new programs as needed. Data were collected and reviewed periodically throughout the monitoring period to assure the integrity of the data.

A wireless link was installed between the As-built tower and the Retrofit tower several miles away. This can be seen in Figure 2.6. Data download from the Retrofit tower was also performed using the satellite uplink.

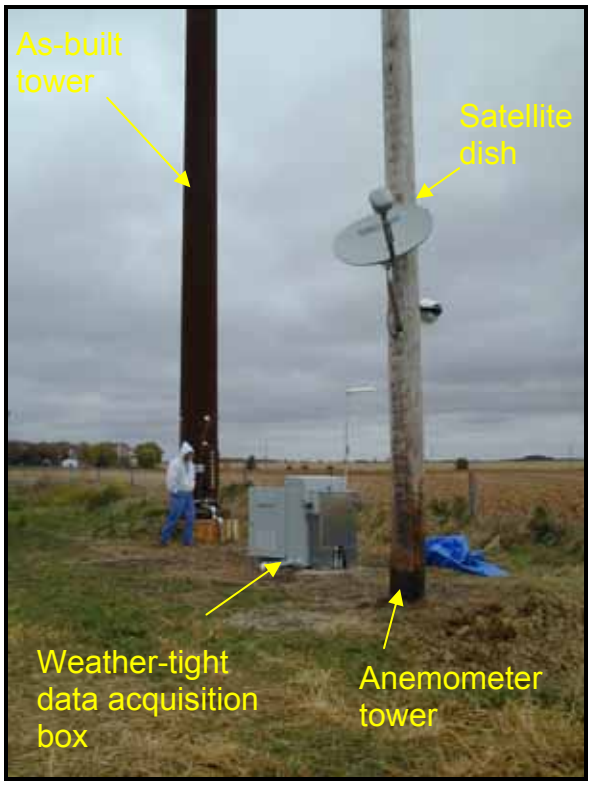

Figure 2.5 – View of As-built tower along I-35 in Clear Lake

Figure 2.6 – View of data acquisition box at As-built tower along I-35 in Clear Lake, IA

2.4.2 Retrofit Tower – Clear Lake

A Campbell Scientific CR5000 data logger was used at the Retrofit tower. This logger is also a high speed, multi-channel 16-bit data acquisition system, however it does not have on-board digital and analog filtering unlike the CR9000. The data logger was enclosed in a weather-tight box adjacent to the tower (see Figure 2.7). A photograph of the inside of the box is shown in Figure 2.8. Constant 120 VAC power was supplied for the duration of the monitoring, though power was interrupted due to a GFCI which tripped occasionally.

Figure 2.7 – View of data acquisition box at the Retrofit tower along US-18 in Clear Lake, IA

Figure 2.8 – View inside the weather-tight box at the Retrofit tower along US-18 in Clear Lake, IA

2.4.3 Dynamic and Static Testing

A CR9000 logger was also used during all static/dynamic testing at the remaining towers tested throughout the State. The data logger was set up in a field vehicle on site. Real-time data were viewed while on site by connecting the data logger directly to a laptop computer. This was done to assure that all sensors were functioning properly.

2.5 Instrumentation Plans

2.5.1 As-built Tower – Clear Lake

A total of fourteen strain gages were installed on the As-built tower at Clear Lake around the base. At two elevations, two orthogonally oriented accelerometers were installed (for a total of four accelerometers). Complete instrumentation plans for the As-built tower at Clear Lake are presented in Appendix A.

2.5.2 Retrofit Tower – Clear Lake

At the Retrofit tower at Clear Lake, six strain gages were installed: two at the base of the jacket, two near the top of the jacket, and two on the tube wall of the tower just above the jacket. Complete instrumentation plans can be found in Appendix A.

2.5.3 Sioux City Towers

As described above, two towers at the I-29/US20 interchange in Sioux City, IA were instrumented. One tower (termed the "As-built" tower) was similar to the tower that collapsed in 2003. The other (termed the "Retrofit" tower) was retrofitted with a more substantial base section. The instrumentation plans for the two poles were nearly identical so meaningful comparisons could be made.

Strain gages were placed at various heights along the tower in addition to selected positions around the circumference. Other gages were placed inside and outside the original tower wall (back-to-back gages) directly above the toe of the column-to-baseplate weld, and at three different locations. These were placed on the side of the tower that experienced maximum tensile stresses during the controlled-load tests. Gages were only placed on the outside of the retrofitted tower due to the fact that it was inaccessible. Locations of the strain gages for the As-built tower are presented in Figure 2.9. The dimension "H" indicated in the Figure represents the height of the strain gages above the base plate. Similar drawings for the Retrofit tower are presented in Figure 2.10. Complete instrumentation plans are presented in Appendix A. A photograph of the base of the two instrumented towers is shown in Figure 2.11.

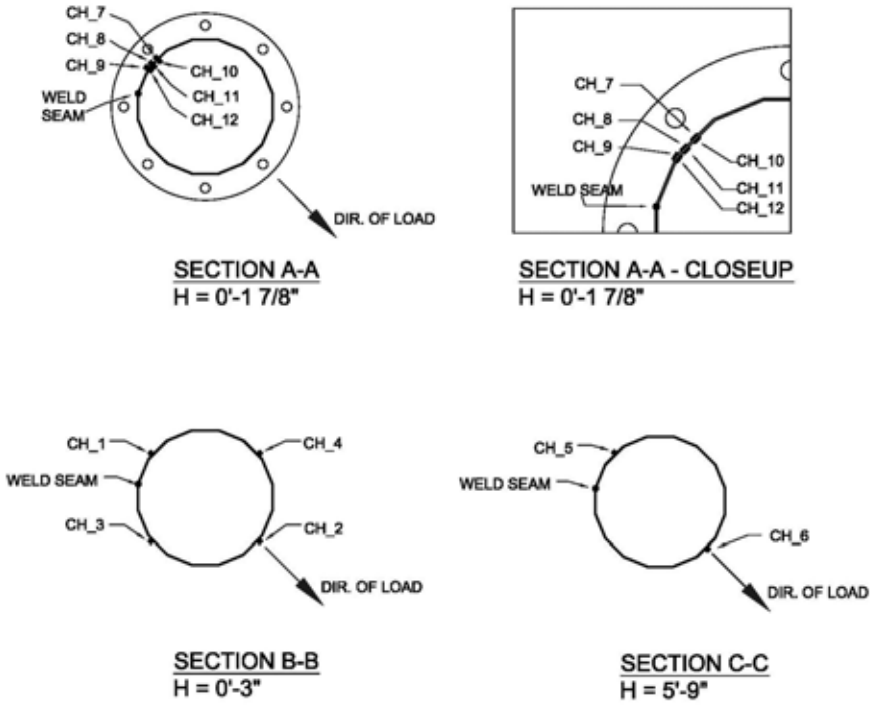

Figure 2.9 – Strain gage details for the As-built tower along I-29 in Sioux City, Iowa

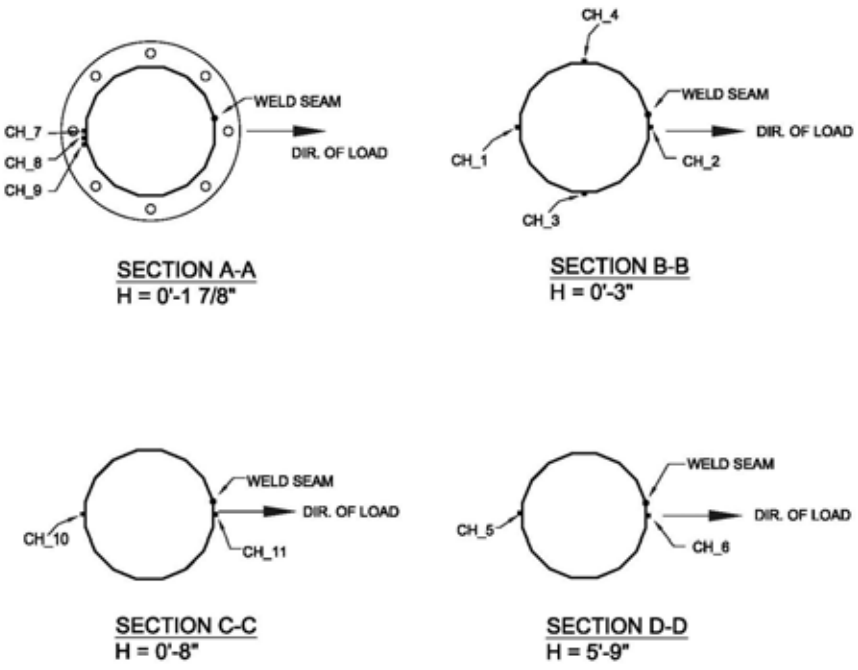

Figure 2.10 – Strain gage details for the Retrofit tower along I-29 in Sioux City, Iowa

(a) As-built tower (b) Retrofit tower

Figure 2.11 – Instrumented high-mast lighting towers at the I-29/US-20 interchange in Sioux City, Iowa

2.5.4 Dynamic Tests

For the dynamic (or "pluck") tests, the instrumentation plan was the same for each test. Two accelerometers, identical to those described in Section 2.2 were clamped to the tower 35 feet above the base plate. One accelerometer was oriented parallel to the applied load, while the other was perpendicular to the load. A typical installation was shown in Figure 2.2.

3.0 Results of Dynamic and Static Testing

3.1 Dynamic Tests

The raw time-history data collected are time-domain signals composed of many sinusoidal components. Using the fast Fourier transform (FFT), a mathematical algorithm, the raw data recorded in the time domain can be transformed into the frequency domain, from which the natural frequencies of the first four modes for each tower can be determined using the "peak picking" method. In general, the natural frequencies of each tower and each mode are within the same range and are also in agreement with values determined by finite element analysis. The first four modal frequencies varied between 0.25 and 7.3 Hz

Three different methods were used to determine the damping ratios of the high-mast light structures; one using pluck test data, and the other two using ambient vibration data. The first method, which utilizes the pluck test data, is the log-decrement (LD) method. In this method, the raw data are subjected to a band-pass filter around a modal frequency, removing all frequencies below and above the frequency of interest, to obtain a free decay profile for a single mode of vibration. From this free decay profile (an example of which is shown in Figure 3.1a), a graph of the natural log of the ratio of successive peaks (equal to δ) is obtained using the following equation:

$$\delta_i = \ln\left(\frac{v_{peak_1}}{v_{peak_i}}\right) \qquad \text{Eqn. 3.1}$$

where i is the cycle number, and v_{peaki} is the peak value of the decrement at cycle i.

An example plot of δ versus cycle number is shown in Figure 3.1b. A best-fit line is determined using least squares. The slope of this line is equal to δ, and can be used to calculate the damping ratio using the following formula:

$$\xi = \frac{\delta}{\sqrt{4\pi^2 + \delta^2}} \qquad \text{Eqn. 3.2}$$

For the example shown in Figure 3.1, δ was found to be 0.2297. Using Equation 3.2, ξ is found to be equal to 3.7%.

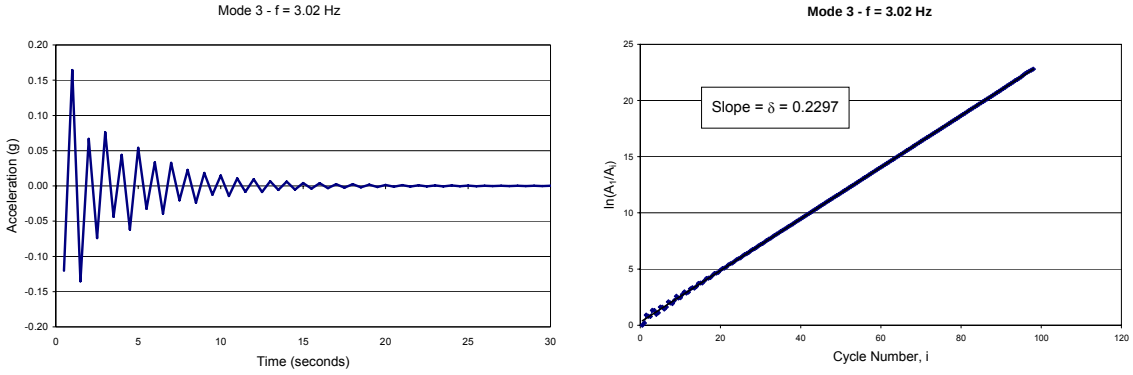

(a) Free Decay Profile (b) Best Fit Line

Figure 3.1 – Log decrement (LD) method

The second method, called the half-power bandwidth method (HPBW), estimates the damping ratio from ambient vibration data using the response in the frequency domain (created by the FFT). Ambient vibration is random vibration caused by natural wind. The damping ratio is calculated using two half-power points that fall on either side of the maximum response peak, and are equal to the peak value divided by the square root of two (see Figure 3.2). The damping ratio, ξ, is calculated from frequencies at the two half-power points using the following formula:

$$\xi = \frac{f_2 - f_1}{f_1 + f_2} \qquad \text{Eqn. 3.3}$$

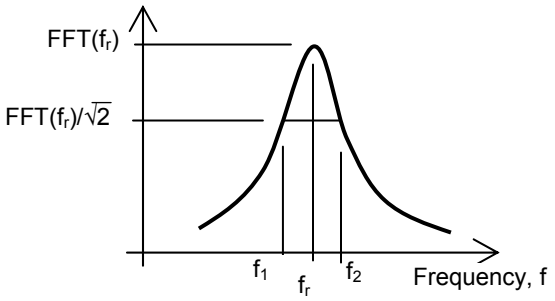

Figure 3.2 – Half-power bandwidth method – definition of half-power points

The third method, the random decrement method (RD), works in the time domain, and also utilizes ambient vibration data. The data are filtered about the modal frequency and a random decrement profile is created by averaging suites of time-history data together selected based on predefined trigger condition using the following equation:

$$\hat{D}_{XX}(\tau) = \frac{1}{N}\sum_{i=1}^{N} x(t_i + \tau)\Big|T_{x(t_i)} \qquad \text{Eqn. 3.4}$$

where D_{xx} is the random decrement signature, x(t) is the acceleration time-history, N is the number of triggers, and $T_{x(t)}$ is the trigger condition.

The random decrement signature is similar to that of a structure in free decay (e.g., Figure 3.2a), and the damping ratio is then similarly calculated using the log-decrement equations discussed above.

Plots of frequency versus the damping ratio of all the towers are shown in Figure 3.3. Also included in the plot are the specified damping ratios from the AASHTO and the CAN/CSA specifications. AASHTO recommends using a ratio of 0.5% when the actual damping ratio of the structure is unknown [2], and the Canadian Bridge Code (CAN/CSA) specifies a damping ratio of 0.75% when experimentally determined values are unavailable [3][4]. These plots show that the damping ratios in all four modes are in many instances considerably lower than the assumed values in the two different codes. Furthermore, the AASHTO and CAN/CSA specifications do not address the possibility of different damping ratios in the higher modes of vibration. These recommended damping ratios are not conservative estimations for the higher modes based on this research.

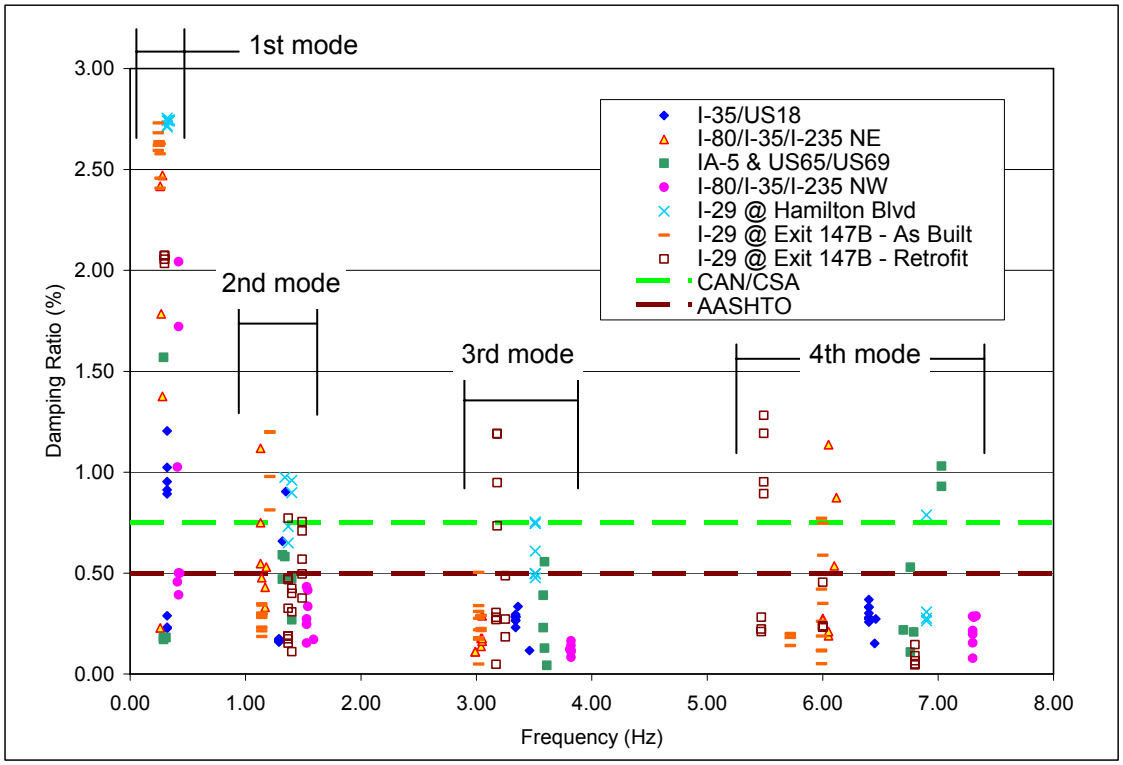

Figure 3.3 – Damping Ratio vs. Frequency

The damping ratios in the first mode, on average, are considerably higher than the other modes. This increase could be attributed to the presence of aerodynamic damping, though it has not been confirmed. Aerodynamic damping is a function of wind speed and is additive with the inherent structural damping of the tower. Aerodynamic damping increases with increasing wind speed.

Structures with high damping ratios require fewer cycles for the vibration to attenuate. The high-mast towers have very low damping ratios and as a result experience a high number of cycles that can cause damage. These cycles can be accumulated during vortex shedding or following natural wind gusts. When a tower with low damping ratios is stressed beyond the constant amplitude fatigue limit (CAFL), a significant number of damaging cycles are accumulated before the stress range falls below the CAFL. The pole-to-base connection of these structures is assumed to be an E' fatigue detail per the code (but may be even worse), with a CAFL of 2.6 ksi, which means that low stress ranges can exceed the CAFL. Therefore, the low CAFL in combination with a low damping ratio can produce many damaging cycles on the high-mast light structures and consequently reduce the fatigue life. However, it should be noted that the designation of E' for the base plate connection is based on a very limited number of tests. It is likely that the actual fatigue performance of these connections is even worse than E' due to the thin baseplates and tube walls found on may high-mast towers.

3.2 Dynamic Analysis

Prior to performing the field tests, a modal analysis of the As-built tower was performed to determine the mode shapes, frequencies and stress distribution. ABAQUS was used as a solver. The tapered tower was modeled using a series of prismatic beam elements, each 2 feet in length. The anchor bolts were modeled as tension/compression elements (the base was fixed from horizontal translation), and were connected to the base using rigid links. A point mass representing the luminaire is located at the top of the tower. The modal analysis included non-linear geometry and included gravity.

Figure 3.4 contains the mode shapes for the first four modes. As shown, the frequencies vary from 0.33 Hz for the first mode, to 6.64 Hz for the fourth mode. Shown in Figure 3.5 is the modal stresses for the first four modes of vibration from the analysis. It is important to note that the magnitudes of the stresses are not meaningful since the stresses are a function of the amplitude of the vibration. These stresses are simply represent a "stress distribution shape." As can be seen in the stress plot for the first mode, the stresses are fairly uniform up the height, which indicates an efficient design.

Comparing the results of the analysis to the test results (Figure 3.4), it can be seen that the frequencies determined by analysis are very close to the measured values.

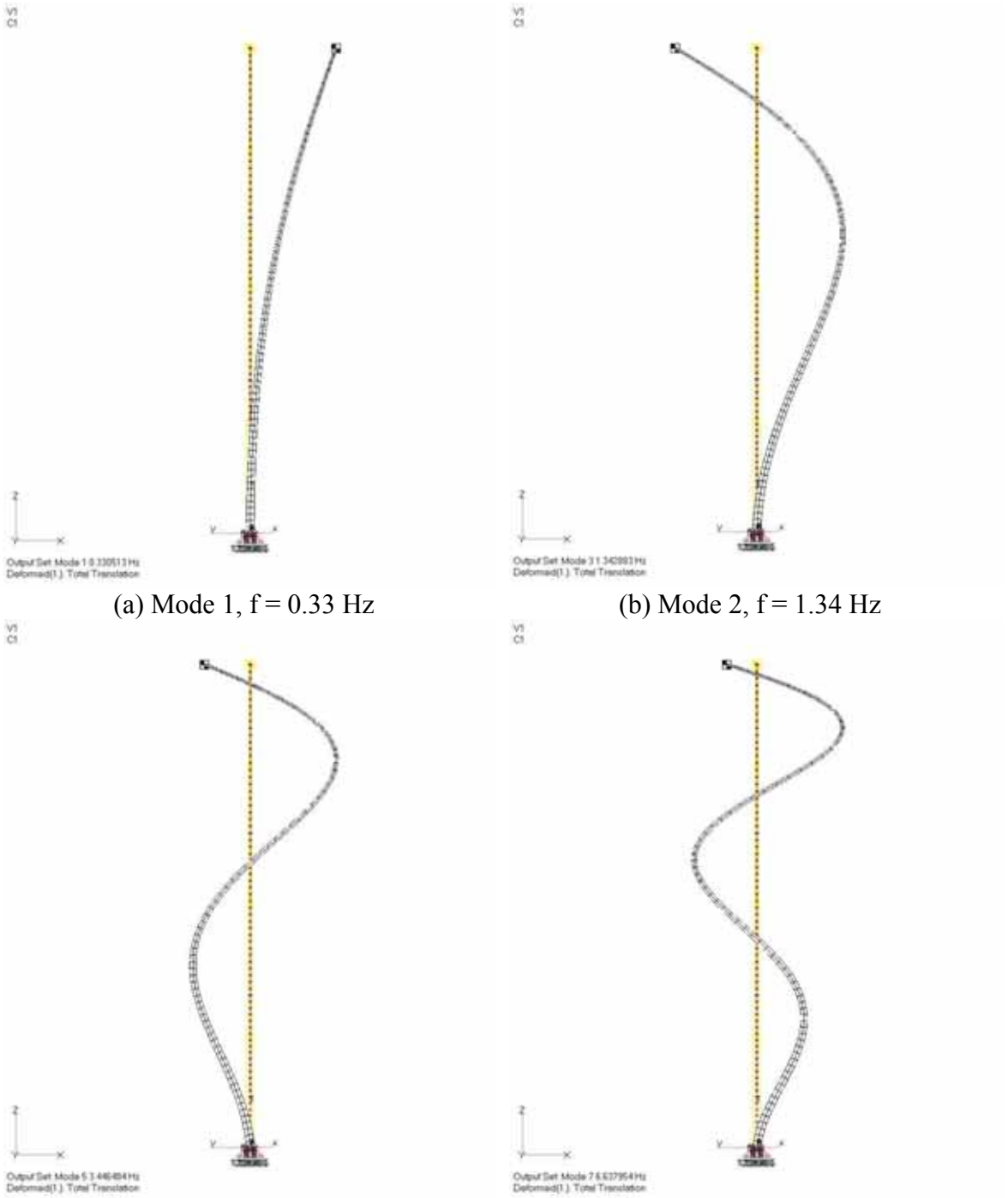

(a) Mode 1, f = 0.33 Hz

(b) Mode 2, f = 1.34 Hz

(c) Mode 3, f = 3.45 Hz

(d) Mode 4, f = 6.64 Hz

Figure 3.4 – Mode shapes and frequencies for the lowest four modes of the As-built tower along I-35 in Clear Lake, as determined using ABAQUS

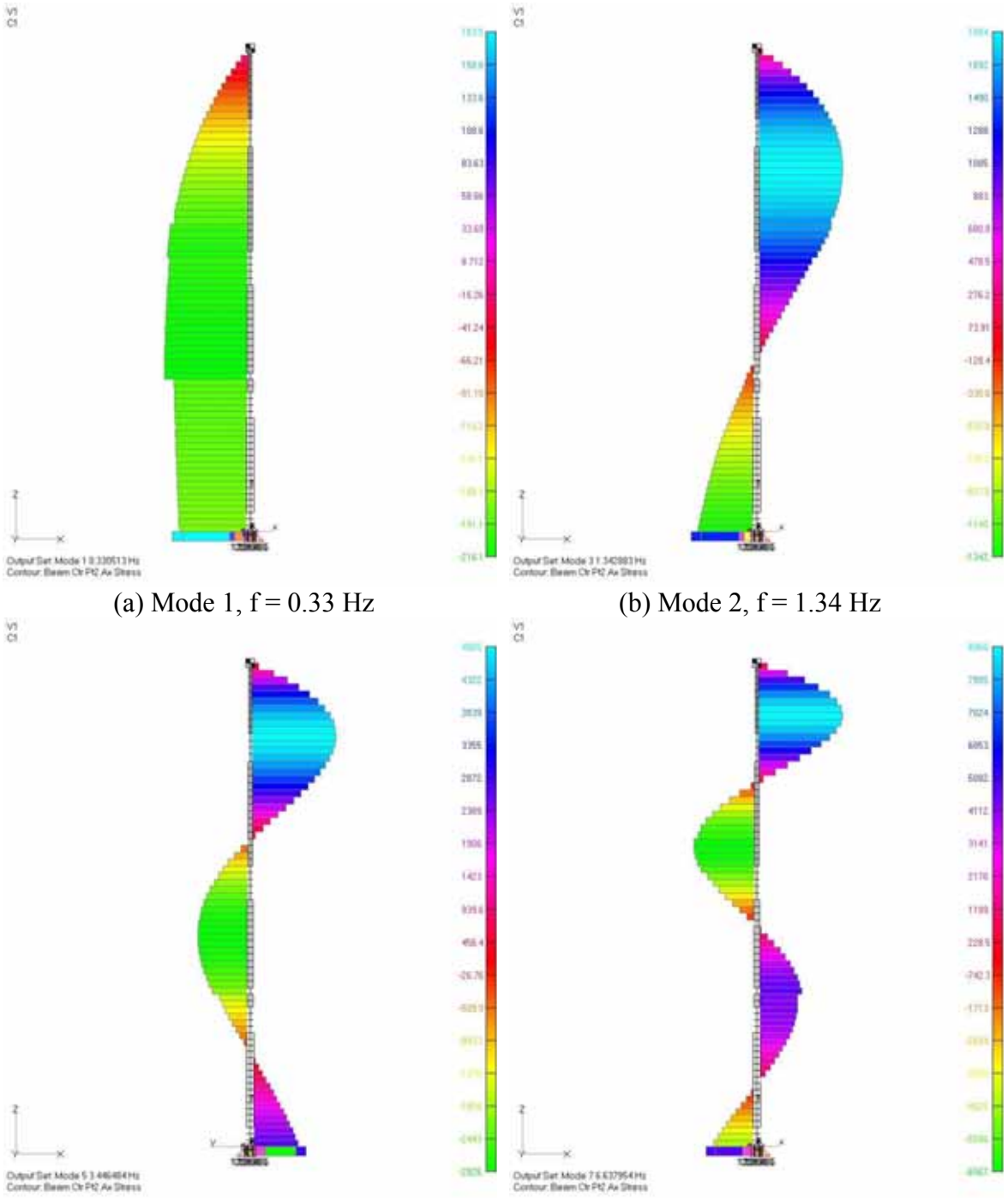

(a) Mode 1, f = 0.33 Hz

(b) Mode 2, f = 1.34 Hz

(c) Mode 3, f = 3.45 Hz

(d) Mode 4, f = 6.64 Hz

Figure 3.5 – Modal stress plots and frequencies for the lowest four modes of the As-built tower along I-35 in Clear Lake, as determined using ABAQUS

3.3 Static Tests

The following section will present the results of static tests that were performed on towers in Sioux City in May 2005 as part of Phase 2 of the field instrumentation efforts. The tests were conducted by first applying a static load by pulling the tower, holding the load, and then suddenly releasing the load forcing the tower into free vibration. The effect of loose and improperly leveled nuts was also examined.

3.3.1 Measured Stresses

The maximum stresses (at selected critical gages) for each tower, prior to the release of the load, are summarized in Table 3.1. All tests shown are with all anchor nuts fully tightened (the test was repeated three times at each tower.) Note that the loads presented in the Table are the measured load in the cable which was inclined (the inclination at the two towers was similar).

			h = 3"		h = 5' 9"		h = 8"	
	Test #	Load (lb)	CH_1 (ksi)	CH_2 (ksi)	CH_5 (ksi)	CH_6 (ksi)	CH_10 (ksi)	CH_11 (ksi)
As-built	1	592	3.89	-2.85	4.63	-4.36	-	-
	2	618	4.63	-3.51	5.51	-5.13	-	-
	3	561	3.77	-3.44	4.49	-4.92	-	-
Retrofit	6	563	1.85	-1.76	1.68	-1.66	1.35	-1.37
	7	602	1.90	-2.00	1.77	-1.78	1.63	-1.70
	8	656	2.01	-2.10	1.83	-1.89	1.68	-1.80

Table 3.1 – Maximum measured stresses at critical locations; h is the vertical distance from the baseplate to the centerline of the strain gage
CH_1 & CH_2 are on opposite sides of the pole in-line with the load
CH_5 & CH_6 are on opposite sides of the pole in-line with the load
CH_10 & CH_11 are on the interior of the tower (As-built tower only)

Note that with the exception of CH_10 and CH_11, the gages were placed in identical locations so that a direct comparison can be made. As expected, the retrofit tower experienced significantly lower stresses than the original tower due to the increased base plate thickness, increased tower wall thickness, and the reinforced hand hole detail.

It should be noted that the stresses near the base plate are not the maximum stresses along the height due to shear lag effects. However, the stresses at the fatigue critical base plate connection are considerably higher than the stresses in the tower due to localized stress concentrations.

3.3.2 Effect of Anchor Nut Loosening

Additional tests were performed to study the effects of loose anchor nuts due to poor installation practices or anchor nuts that loosen over time. Three tests were conducted to monitor these effects: two on the original tower and a third on the retrofit tower. During the first test, one nut was loosened, the load was applied and released, then a second nut was loosened, the load was reapplied, and the tower was subsequently plucked. During the second test, a leveling nut was loosened and the top nut was tightened down to simulate the effect of improper leveling of the leveling nuts prior to tightening the top nuts. The third test involved loosening two bolts while the load was applied, and subsequently plucking the tower.

The pluck tests with loose anchor bolts did not significantly alter the damping ratios, as expected. However, it appears that the 1st and 3rd modes were not excited, as determined by an FFT analysis of the raw data. However, localized increases in stress were measured near the baseplate and in the vicinity of the loose anchor nuts, as shown in Table 3.2. During tests number 4 and 9, the anchor nut furthest from the load (extreme tension fiber) was loosened.

			h = 3"		h = 5' 9"		h = 8"	
	Test	**Load (lb)**	**CH_1 (ksi)**	**CH_2 (ksi)**	**CH_5 (ksi)**	**CH_6 (ksi)**	**CH_10 (ksi)**	**CH_11 (ksi)**
As Built	4	n/a	4.74	-2.84	4.09	-3.96	-	-
Retrofit	9	665	7.19	-2.67	1.67	-1.60	3.99	-2.08

Table 3.2 – Maximum measured stresses at critical locations during anchor nut loosening tests

Comparing the stresses measured in the towers with properly (Table 3.1) and improperly (Table 3.2) tightened anchor nuts, it can be noted that the towers with improperly installed anchor nuts are subjected to concentrated stress increases in the vicinity of the loose anchor bolts.

To evaluate the effect of leveling nuts that are not properly leveled prior to final tightening, one leveling nut (adjacent to strain gage CH_1) was purposely lowered approximately 1/8 inch. Data from all strain gages were recorded while the top nut was tightened down. The data from strain gages CH_1, CH_2, CH_7, CH_8, and CH_9 recorded during this operation are presented in Figure 3.6. Each of the plateaus on the strain history represents a break between successive tightening operations. Strain gage CH_1 is located on the tube wall 3 inches above the column-to-base weld toe near the improperly tightened anchor bolt. Strain gage CH_2 is on the opposite face from CH_1. Notice that the stresses on the opposite side of the tower (CH_2) are not affected by the loose anchor bolts.

Strain gages CH_7, CH_8, and CH_9 are located at the weld toe below CH_1 (see Figure 2.9.) It can be seen that at the weld toe, very high stresses (70 ksi) are induced into the tube wall by tightening down the anchor nut. It is likely that the material locally yielded.

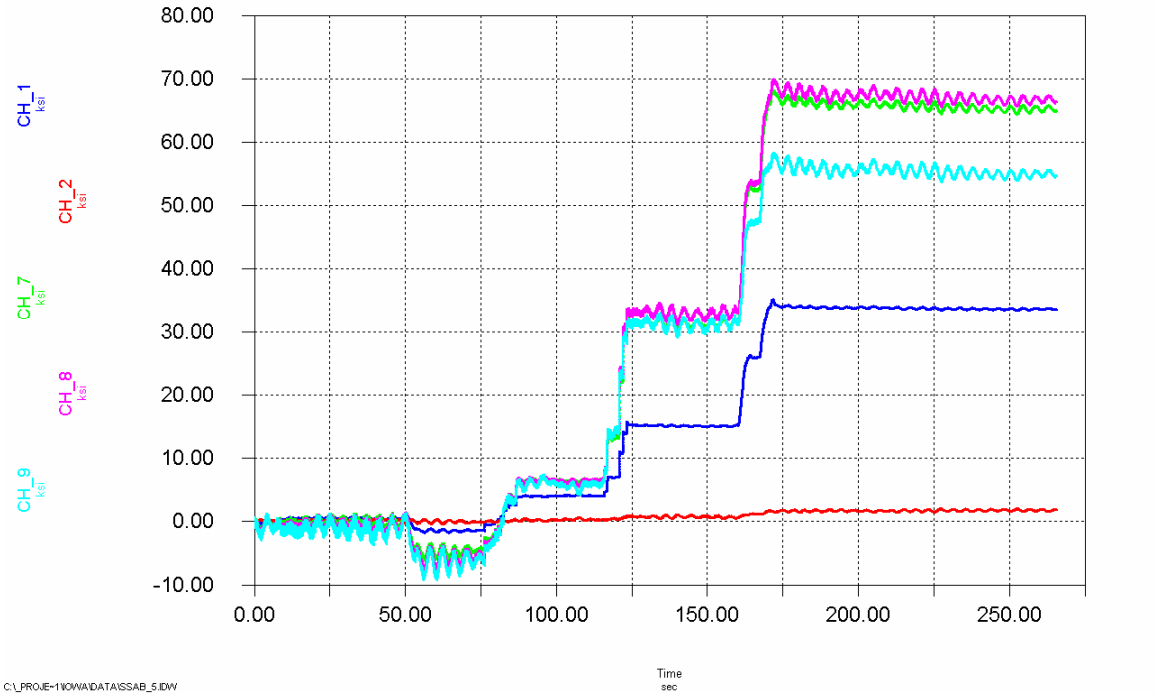

Figure 3.6 – Localized stress changes due to poor installation techniques

4.0 Results of Long-term Monitoring

The results of the long-term monitoring phase of the project will be discussed in this section. As discussed previously, two towers located at the interchange between I-35 and US18 in Clear Lake, Iowa were monitored for a period of one year, specifically from October 15, 2004 to November 5, 2005. The first tower (identified in the design documents as tower #1) was instrumented with 14 strain gages. This tower is in its original as-built condition, and it is uncracked. *(Other cracked towers had been found in this interchange and were taken down).* As noted previously, this tower is referred to as the "As-built" tower in this report.

The second tower (identified as tower #7 in the design documents) is identical but retrofitted with a splice jacket at its base. Six strain gages were installed (four on the jacket, two on the tower directly above the jacket). This tower is referred to as the "Retrofit" tower in this report.

Stress-range histograms were recorded every 10 minutes using the rainflow cycle counting algorithm [7] for the duration of the monitoring period (except during regular maintenance and power outages). These histograms were generated for six selected strain gages on each tower. A stress range histogram is basically a tally of stress cycles of predetermined ranges. Every ten minutes, the data acquisition system updates the tally. A fatigue evaluation of the towers was performed using the stress-range histograms, which were truncated at a level equal to approximately 1/4 of the constant amplitude fatigue limit (CAFL) of the detail in question per AASHTO. That is, all cycles with stress ranges less than the truncation level were removed from the histogram prior to calculation of the effective stress. An in-depth discussion of the methodology used for the fatigue evaluation can be found in Appendix B.

In addition to the stress-range histograms, stress time-history data were recorded when predefined trigger events occurred. These "trigger events" occurred when wind speed and stress events at selected locations exceeded various levels. When a trigger event was detected, data were recorded from all sensors for a predefined length of time. The stress time history data were used to assess the validity of large stress-range cycles recorded in the stress-range histograms, and to understand the wind phenomena that caused them.

Finally, average wind data were recorded continuously at each tower, on a three minute interval at the As-built tower and on a one minute interval at the Retrofit tower. During each interval, the data logger records the average and maximum wind speed, and the average wind speed.

4.1 As-built Tower – Clear Lake

4.1.1 Stress-Range Histograms

Stress-range histograms were developed for six strain gages, as shown in Table 4.1. A total of 347 days of data were collected. Strain gages CH_1 and CH_3 are oriented vertically, 90 degrees apart at the base of the tower, while strain gages CH_10 and CH_12 are oriented vertically, 90 degrees apart at a section 5'-9" above the baseplate. Each of these four gages were centered on a face of the tower (away from the bend lines). Strain gage CH_9 is oriented vertically on the tower at the upper left corner of the handhole. Finally, strain gage CH_11 is oriented vertically 3 inches above the

baseplate directly on a bend line. A detailed instrumentation plan for this tower is contained in Appendix A.

Strain Gage	Location
CH_1	NW side; 3" above baseplate
CH_3	SW side; 3" above baseplate
CH_9	Above left side of hand hole
CH_10	SW side; 5'-9" above baseplate
CH_11	North side at bend; 3" above baseplate
CH_12	NW side; 5'-9" above baseplate

Table 4.1 – Summary of strain gages for which stress-range histograms were developed at the As-built tower

Figure 4.1 contains the measured stress-range histograms for the six strain gages identified above. Note that the highest stress-ranges were recorded at strain gage CH_9, above the hand hole. A fatigue life calculation was performed for each of the gages listed in Table 4.1. The results are presented in Table 4.2.

The socket connection at the base of the tower (strain gages CH_1 and CH_3) is considered at category E' per AASHTO [2], with a CAFL of 2.6 ksi. All stress cycles less than 0.5 ksi were removed from the histogram. The maximum measured stress range in CH_1 was 4.5 ksi, while in strain gage CH_3, it was 7.0 ksi. The CAFL of 2.6 ksi was exceeded at a frequency of 0.04% which is greater than 0.01% (1/10,000), therefore, finite fatigue life can be expected. For these two gages, the minimum calculated fatigue life is equal to 40 years. At strain gage CH_10, the estimated remaining fatigue life is only 10 years. However, it must be noted that the category designation of E' is based on very limited laboratory testing and most likely is unconservative due to the relatively thin tube wall and baseplate. Laboratory testing as part of upcoming NCHRP and pooled fund research projects is planned to improve the existing fatigue knowledgebase on these details. It can be seen that there is a large difference between the effective stress range and the calculated remaining life at gages at the base of the tower (CH_1 and CH_3) and gages 5'-9" above the base (CH_10 and CH_12). The higher stresses are most likely the result of the taper of the pole, or may be due to the fact that gages at the center of the face at the base have reduced stress compared to the stress at the bend line due to the stress concentration there. At the section 5'-9" above the base, the stress concentration is not present.

The handhole detail (strain gage CH_9) is considered a category E detail per the code since its length is greater than 4 inches, with a CAFL of 4.5 ksi. All stress cycles less than 1.0 ksi were removed from the histogram. The calculated fatigue life for this detail is equal to 22 years. However, as with the pole-to-base connection, this category designation is based on very limited testing. The actual performance may be worse due to the large lack-of-fusion zone. If this detail is considered E', the expected remaining life is equal to 3 years (the E' CAFL was exceeded with a frequency of over 3%.)

It can also be seen that there are some very large stress cycles that were induced at several of the gages, namely CH_9 (17.5 ksi) and CH_10 (12.5 ksi) and CH_12 (11.5 ksi). The maximum stresses recorded at each gage were the result of natural wind gusts.

Furthermore, the CAFL of all details (which may be conservative) was exceeded with a frequency of more than 1 in 10,000 at all gages. The stresses caused by vortex shedding were of a much lower magnitude.

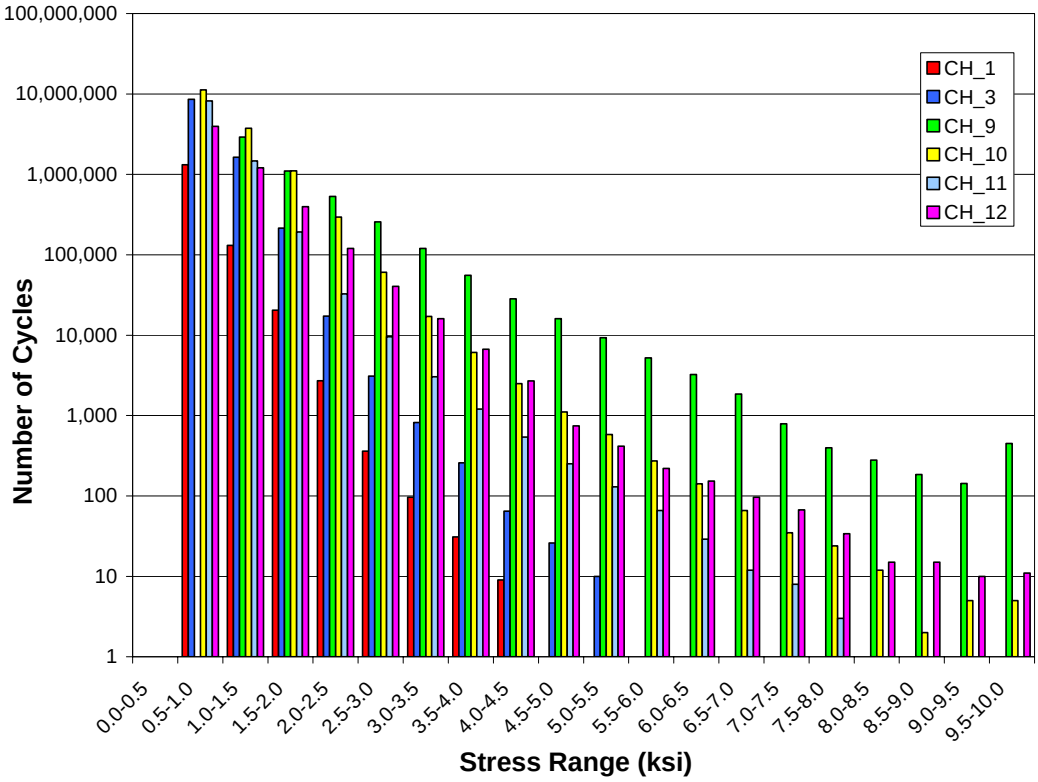

Figure 4.1 – Stress-range histograms for strain gages located on the As-built tower

Strain Gage	Assumed Category (CAFL)	S_{Rmax} (ksi)	Cycles > CAFL		S_{Reff} (ksi)	Cycles/ day	Remaining Life (years)
			#	%			
CH_1	E' (2.6)	5.5	499	0.03%	0.9	4,246	379
CH_3	E' (2.6)	7.0	4,284	0.04%	0.9	30,184	40
CH_9	E (4.5)	17.5*	36,801	0.73%	2.0	14,538	22
CH_10	E' (2.6)	11.5*	88,726	0.54%	1.1	47,496	10
CH_11	E' (2.6)	8.5	14,874	0.15%	0.9	28,646	40
CH_12	E' (2.6)	12.5*	67,498	1.17%	1.2	16,573	33

*S_{Rmax} determined from time-history data

Table 4.2 – Summary of fatigue life calculation for As-built tower

4.1.2 Long-Term Wind Data

A total of 275 days of complete wind data were obtained during the long-term monitoring phase of this project. Wind data were recorded on three minute intervals for the duration of the long-term monitoring (higher speed sampled wind data were recorded when trigger events occurred). Every three minutes, the average wind speed, maximum wind speed, and the average wind direction were recorded. Using these data, trends can be observed in the wind at the site, such as prevailing wind direction, and magnitude of prevailing winds.

Figure 4.2 shows a polar histogram plot for all data collected during the long term monitoring. This plot shows the percent occurrence of winds from all directions in polar form, with zero degrees being north. The plot has two lobes, indicating that most of the time the wind blows from either the northwest, or south-southeast.

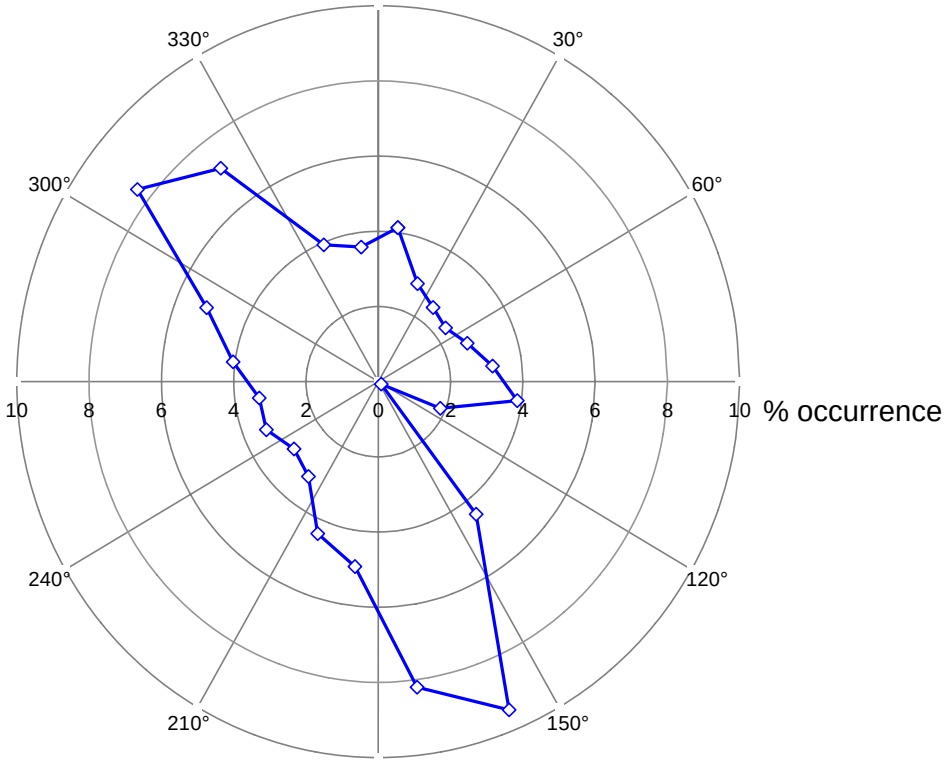

Figure 4.2 – Wind rose for percent occurrence for the As-built tower

Figure 4.3 shows a polar plot of the average wind speed. This plot presents the average wind speed at each direction for the duration of the monitoring period. Again, zero degrees corresponds to north. It can be seen that the highest average wind speeds are approximately 12 mph and generally occur from the same direction as the most frequent wind directions shown in Figure 4.2.

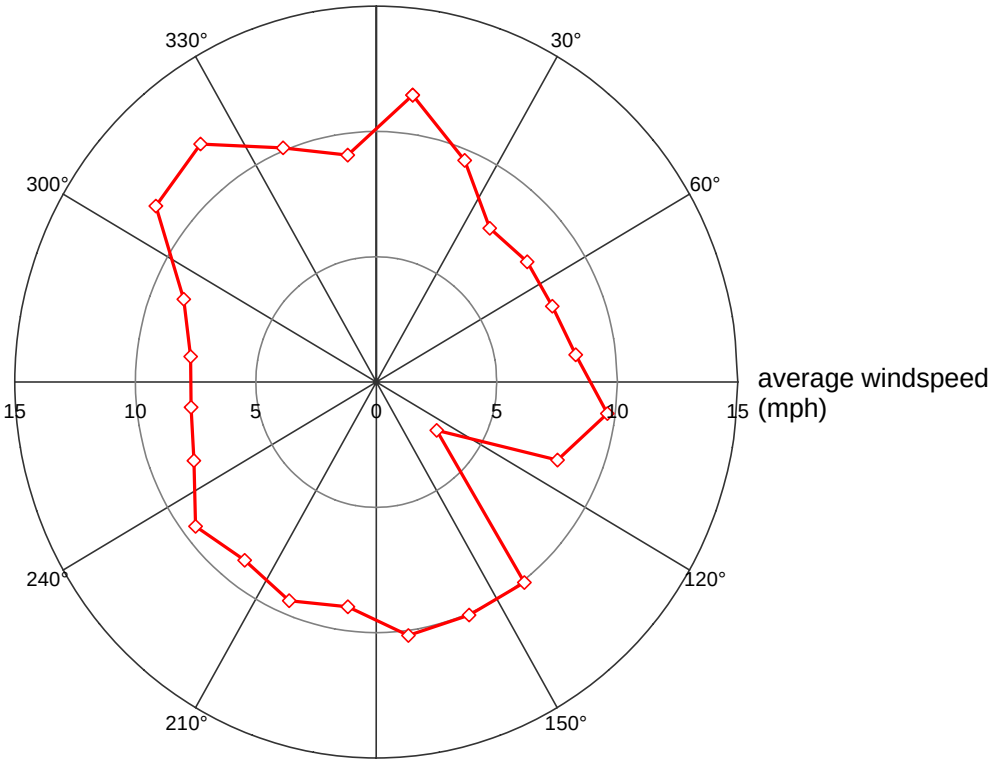

Figure 4.3 – Wind rose of average wind speed for the As-built tower

A plot of the average and peak daily wind speeds for the As-built tower is shown in Figure 4.4. It can be seen that the peak wind speed recorded during the monitoring period was 58 mph recorded on May 8, 2005. It is also noted that the wind speed regularly exceeds 30 mph.

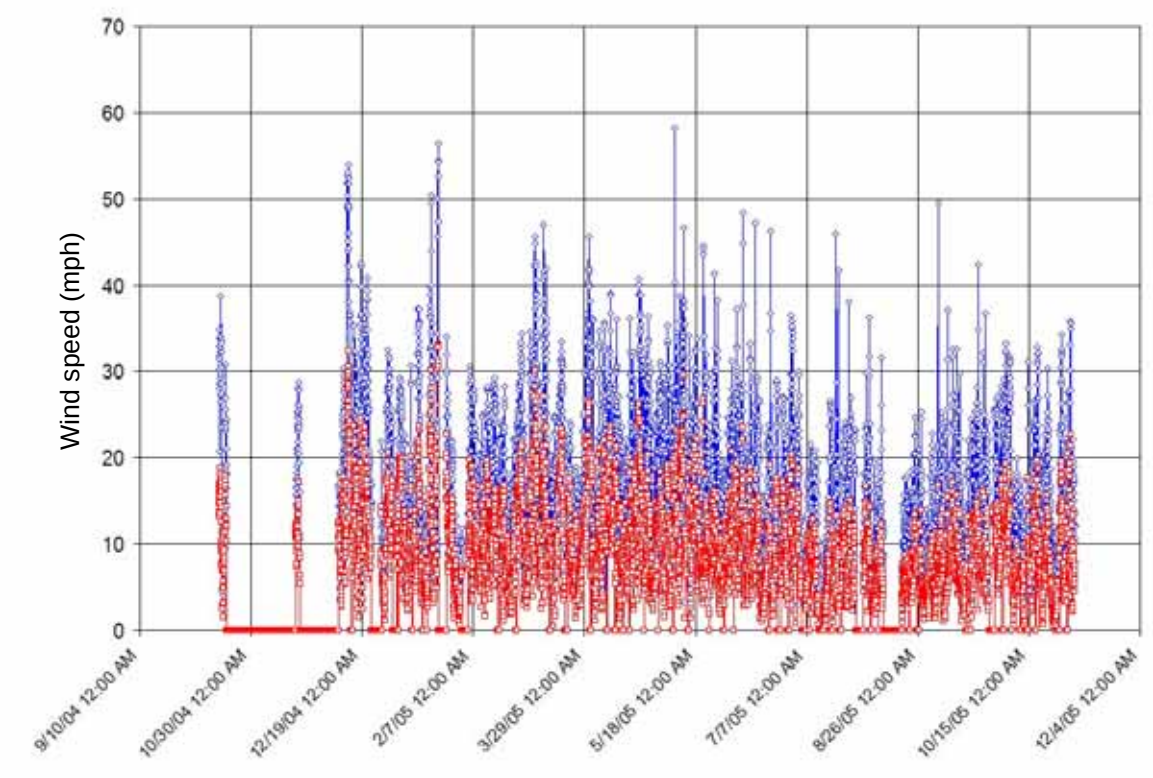

Note: Average daily wind speed is plotted in red
Maximum daily wind speed is plotted in blue

Figure 4.4 – Wind speed history for As-built tower

4.2 Retrofit Tower – Clear Lake

4.2.1 Stress-Range Histograms

Stress-range histograms were developed for five strain gages, as shown in Table 4.3. A total of 78 days of data were collected. The reduced quantity of data collected at the Retrofit tower was the result of several factors. First, power was frequently lost at the site. During a visit to the tower in May 2005, water was found inside the data acquisition enclosure box. Furthermore, there was electrical noise found in the data which corrupted the stress-range cycle counting. The 78 days of data reported herein are free from noise and can therefore be used for a fatigue evaluation of the tower.

All strain gages are oriented vertically. Gage CH_2 is located on the base of the jacket. Gages CH_3 and CH_4 are located near the top of the jacket on opposite sides. Finally gages CH_5 and CH_6 are located on the tower just above the jacket on opposite sides. Each of these gages were centered on a face of the tower (away from the bend lines). A detailed instrumentation plan for this tower is contained in Appendix A.

Strain Gage	Location
CH_2	West base of jacket, 3” above baseplate
CH_3	East side of jacket; 4.75” down from top
CH_4	West side of jacket; 4.75” down from top
CH_5	East side of tower 6” above jacket
CH_6	West side of tower 6” above jacket

Table 4.3 – Summary of strain gages for which stress-range histograms were developed at the Retrofit tower

Figure 4.5 contains the measured stress-range histograms for the five strain gages identified above. Note that the highest stress-ranges were recorded at strain gages CH_5 and CH_6, above the splice jacket. A fatigue life calculation was performed for each gage. The results are presented in Table 4.4.

The full penetration weld at the base of the tower (strain gage CH_2) is considered at category E’ per AASHTO [2], with a CAFL of 2.6 ksi. (It is noted CH_2 is located on the jacket and not on the original tower wall.) All stress cycles less than 0.5 ksi were removed from the histogram. The maximum measured stress range in CH_2 was 6.5 ksi. The CAFL was exceeded at a frequency of 0.02% which is greater than 0.01% (1/10,000), therefore, finite fatigue life can be expected. However, for this strain gage, the minimum calculated fatigue life is greater than 100 years, or effectively infinite life.

Strain gages CH_3, CH_4, CH_5, and CH_6 are installed at locations considered to be fatigue category B for a slip-critical bolted connection, with a CAFL of 10 ksi. As a result, all stress cycles less than 2.5 ksi were removed from the spectrum. It can be seen from Table 4.4 that the CAFL was never exceeded and therefore infinite fatigue life can be expected on the jacket itself.

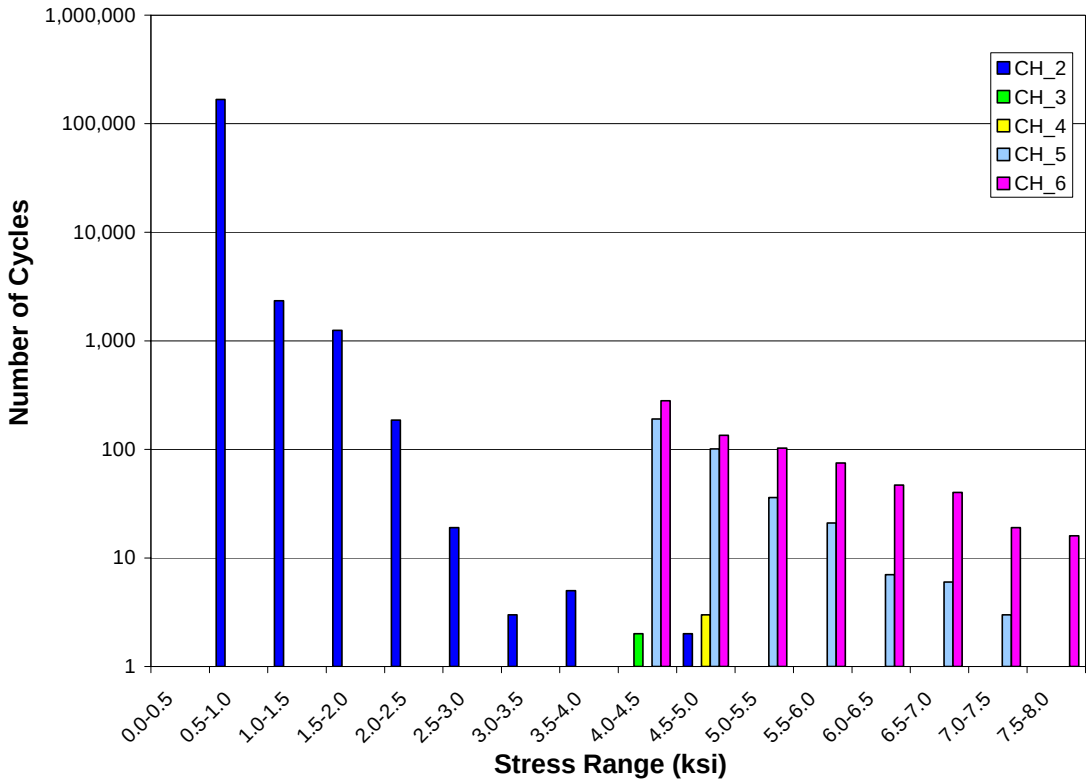

Figure 4.5 – Stress-range histograms for strain gages located on the Retrofit tower

Strain Gage	Assumed Category (CAFL)	S_{rmax} (ksi)	Cycles > CAFL		S_{reff} (ksi)	Cycles/ day	Remaining Life (years)
			#	%			
CH_2	E' (2.6)	6.5	33	0.02%	0.8	2,206	>100
CH_3	B (16)	5.0	0	0.00%	4.3	0	Infinite
CH_4	B (16)	5.0	0	0.00%	4.8	0	Infinite
CH_5	B (16)	7.5	0	0.00%	4.8	5	Infinite
CH_6	B (16)	9.4*	0	0.00%	5.3	9	Infinite

*S_{Rmax} determined from time-history data

Table 4.4 – Summary of fatigue life calculation for the Retrofit tower

4.2.2 Long-Term Wind Data

A total of 63 days of complete wind data (including direction) were obtained at the retrofit tower during the long-term monitoring phase of this project. A smaller quantity of wind data were collected at the Retrofit tower (compared to the As-built tower) for the same reasons cited above, i.e., loss of power and electrical noise in the data. The data presented herein (representing a total of 63 non-consecutive days) are free from noise and are of good quality. Wind data were recorded on one minute intervals for the duration of the long-term monitoring (higher speed sampled wind data were recorded when trigger events occurred). Every minute, the average and maximum wind speed (at all three anemometers), and the average wind direction (bottom anemometer only) were recorded. Using these data, trends can be observed in the wind at the site, such as prevailing wind direction, and magnitude of prevailing winds.

Figure 4.6 shows a polar histogram plot for all data collected during the long term monitoring. This plot shows the percent occurrence of winds from all directions in polar form, with zero degrees being north. The plot has two lobes, indicating that most of the time the wind blows from either the northwest, or south-southeast. It can be seen that the shape of the plot is very similar to that presented in Figure 4.2 for the As-built tower as expected.

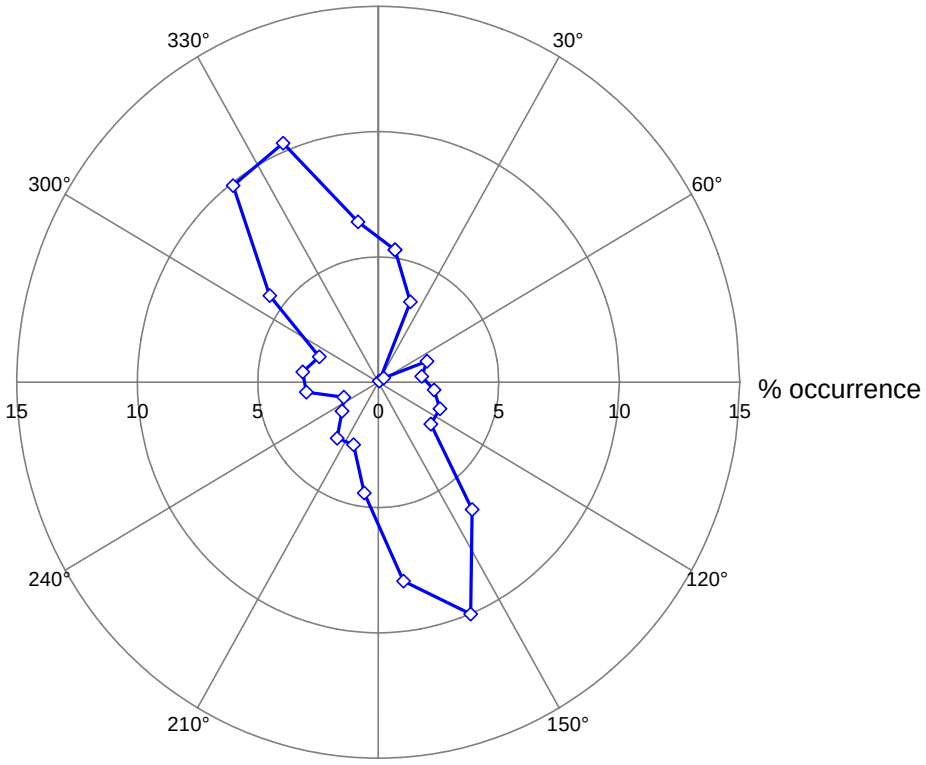

Figure 4.6 – Wind rose for percent occurrence for the Retrofit tower

Figure 4.7 shows a polar plot of the average wind speed. This plot presents the average wind speed at each direction for the duration of the monitoring period. It can be seen that the highest average wind speeds are approximately 23 mph and generally occur from the same direction as the most frequent wind directions shown in Figure 4.6. The average wind speeds are higher than those recorded at the As-built pole.

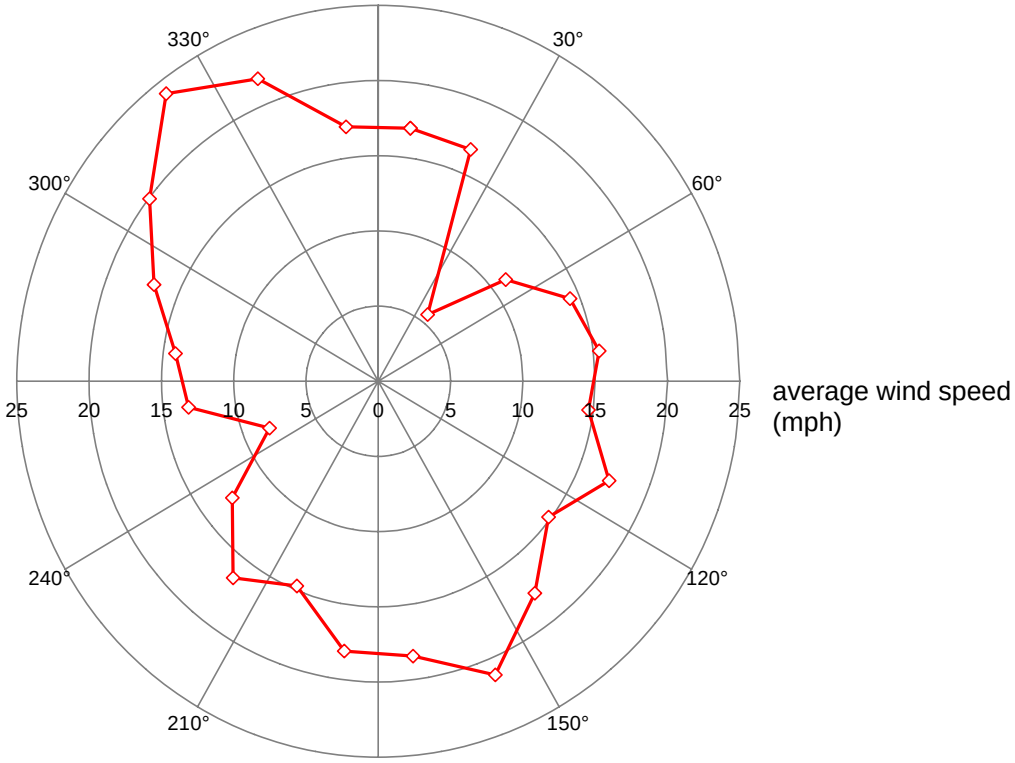

Figure 4.7 – Wind rose of average wind speed for the Retrofit tower

Presented in Figure 4.8 is a histogram plot of the ratios of average hourly wind speed. One line represents the ratio of average hourly mid-height wind speed to average hourly base wind speed. The second line represents the ratio of average hourly top wind speed to average hourly base wind speed. A similar plot for maximum hourly wind speed is shown in Figure 4.9. On these plots, a value of 1.0 denotes that the wind speed (either top or mid-height) is equal to the base wind speed. When the value is less than one, the top or mid-height wind speed is less than that at the base.

Every hour of data, the average and maximum wind speeds are determined at the base, mid-height, and top anemometers which were installed on the Retrofit tower (see Figure 2.3.) For each hour, the ratio of top and mid height wind speeds (both maximum and average) are calculated. A histogram is then determined separately for the average Figure 4.8) and maximum (Figure 4.9) quantities for the entire data set based on the wind speed at the base. It can be seen in the plots that for low wind speeds (i.e., less than 10 mph), the wind speeds at the top are high than the base (approximately 1.5 times higher) but the wind speeds at mid-height are actually less than the wind speed at the base. This

may be due to the local terrain at the tower . The tower is located in a depression, and may be subject to local wind effects.

As the wind speed increases, the top and mid-height wind speeds appear to approach each other, leading to a uniform wind speed distribution from the mid-height and upwards. However, both these wind speeds are less than the average base wind speed; the ratios are approximately 0.8 for both average and maximum wind speed. To confirm this effect, and validate the accuracy of the anemometers, they will be recalibrated upon retrieval from the field.

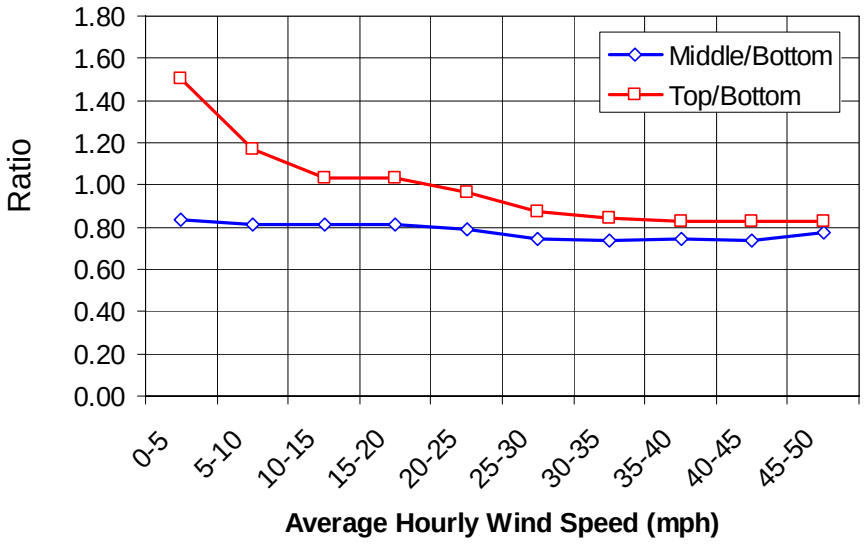

Figure 4.8 – Histogram of average hourly wind speed ratios, mid-height/base and top/base for the Retrofit tower

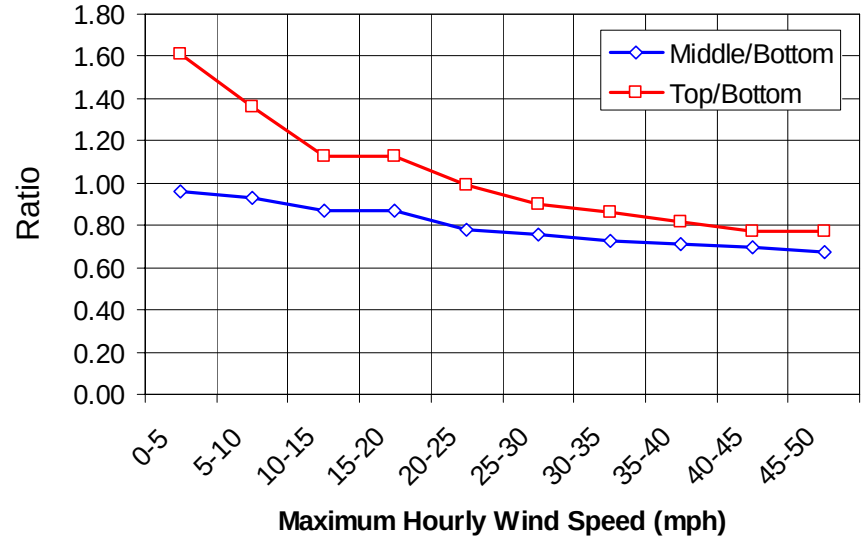

Figure 4.9 – Histogram of maximum hourly wind speed ratios, mid-height/base and top/base for the Retrofit tower

4.3 Natural Wind Gusting

In this section, a high-wind event which occurred during the long-term monitoring phase of the project will be examined. During this event, natural wind gusts excited the towers and caused large stress ranges. Figure 4.10 shows wind speed and direction time histories for a high-wind event which occurred on January 22, 2005 at 5:20 AM. It can be seen that at the beginning of the event, the wind speed varies between 20 and 30 mph, but then at time 700 seconds, the wind speed starts to increase to a maximum of 55 mph. Also note that the wind speed during this entire event is fairly constant, ranging between 280 and 340 degrees, one of the primary wind directions presented in the wind rose plots of Figures 4.2 and 4.3. At time equal to 792 seconds, it can be seen that a large gust occurred during which the wind speed rapidly increased from 25 mph to 50 mph in a matter of 5 seconds. This loading rate is close to the first natural frequency of 0.3 Hz (or a vibration period of 3.3 seconds).

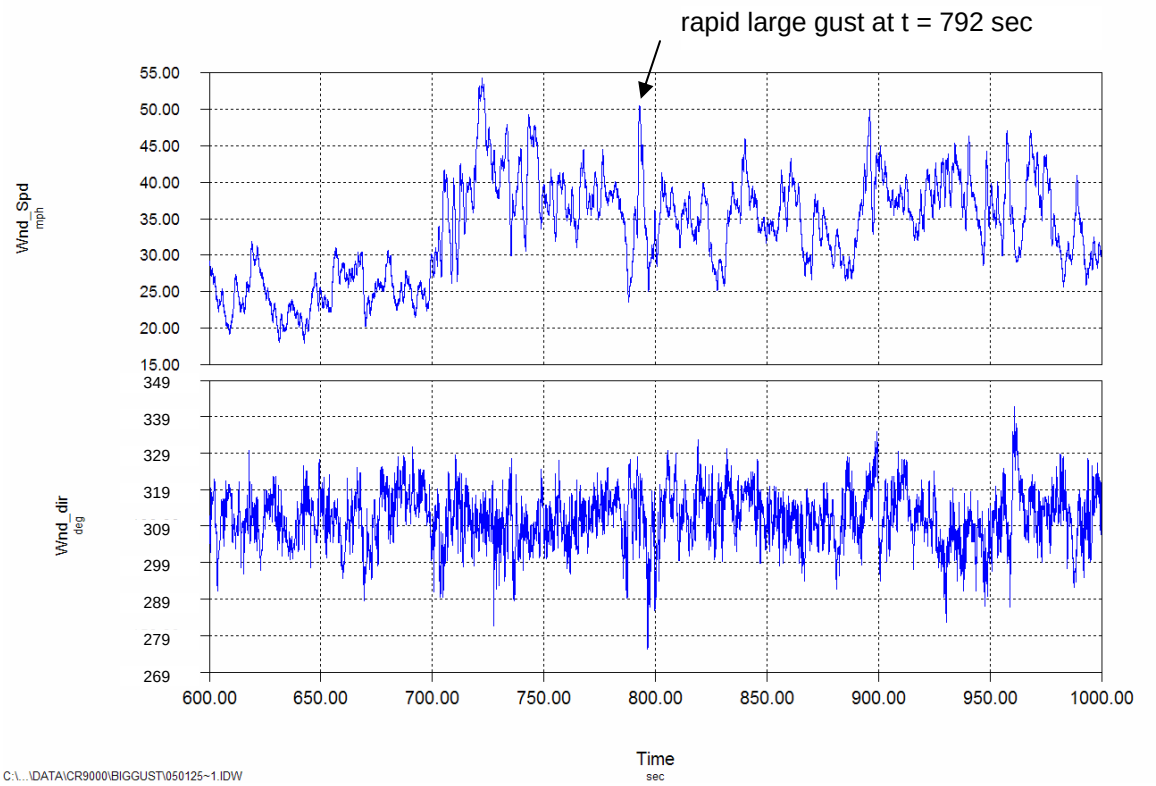

Figure 4.10 – Wind speed and direction time-histories for a large wind event at the As-built tower on January 22, 2005 and 5:20AM

Shown in Figure 4.11 is a stress time history for the rapid gust event discussed above. Strain gages CH_3 and CH_4 are on the west and east sides of the pole, respectively, 3 inches above the base. Strain gages CH_10 and CH_13 are on the west and east sides of the pole, respectively, 5 feet 9 inches above the base. The response at all strain gages was relatively low (less than 2 ksi) until the large gust occurred at time equal to 792 seconds, at which point the stresses in all gages rose dramatically (maximum of 6.2 ksi at CH_10). Primarily the response was in the first vibration mode, as the time between successive peaks was approximately 3.3 seconds. It can also be seen that the vibration of the pole continued for a number of cycles after the original event. These additional stress cycles contribute to the cumulative fatigue damage at the base of the tower.

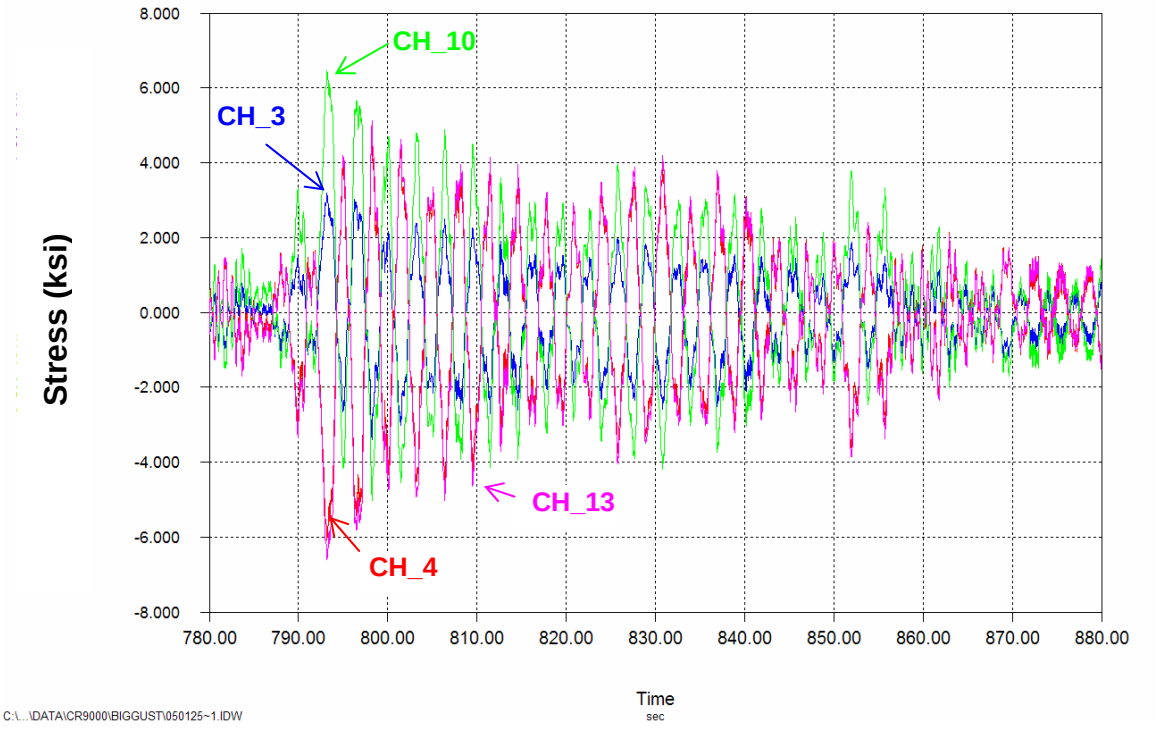

Figure 4.11 – Stress time-history for four gages on the east and west sides of the tower for a large wind event at the As-built tower on January 22, 2005 and 5:20AM

Figure 4.12 shows a stress time-history for three adjacent gages (CH_8, CH_11 and CH_6) for the same high-wind event. Gages CH_6 and CH_8 are centered on two adjacent faces of the tower (away from the bend line). Gage CH_11 is located on the bend line between gages CH_6 and CH_8. All gages are located 3 inches above the base. It can be seen that in general, the magnitude of stress on the bend line appears to be between the stress at the two adjacent faces.

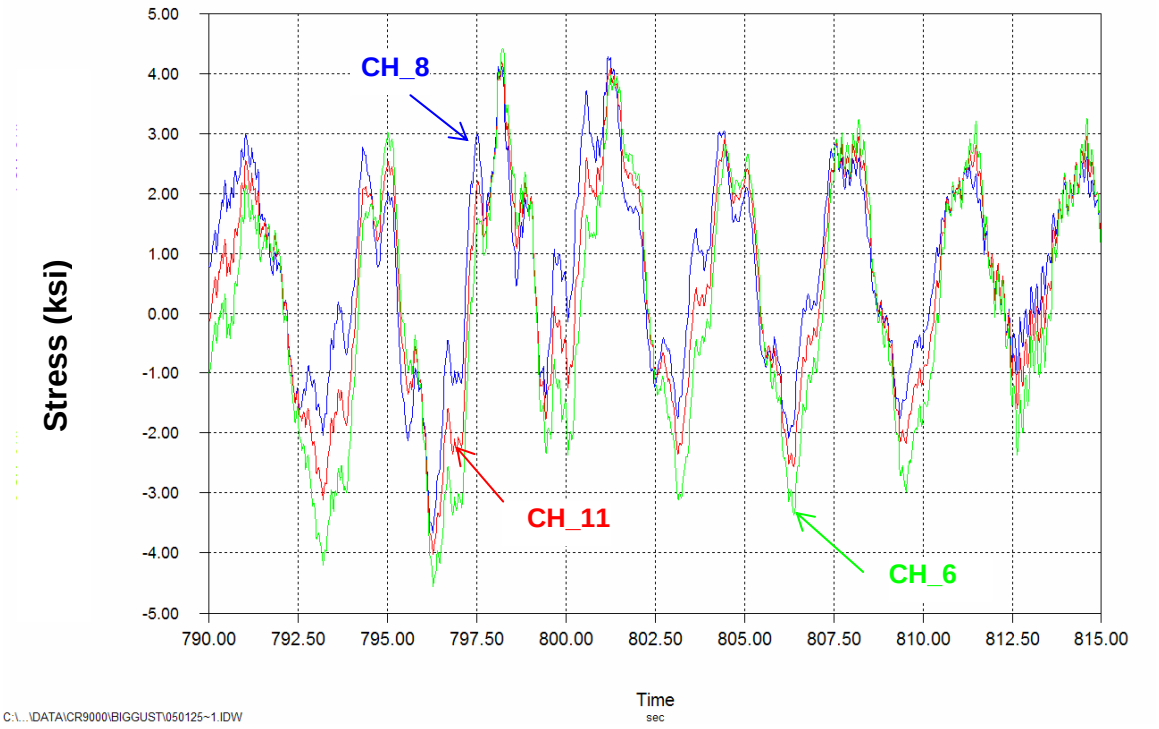

Figure 4.12 – Detailed stress time-history for a large wind event
at the As-built tower on January 22, 2005 and 5:20AM

Finally, Figure 4.13 contains a stress time-history for the same wind event, for strain gages CH_9 and CH_14. Gage CH_9 is above the hand hole, while CH_14 is several feet above the hand hole on the same face of the pole. It can be seen that the stress histories are similar except that the stress at the hand hole (CH_9) is higher due to the stress concentration there. Furthermore, the Figure indicates that the stress range at the hand hole is very high, equal to 14.1 ksi. This was also evident from the stress-range histogram shown in Figure 4.1. Again, it was found that during the long-term monitoring phase of the project, that the largest stress ranges were caused by natural wind gusting, and the response was primarily in the first mode.

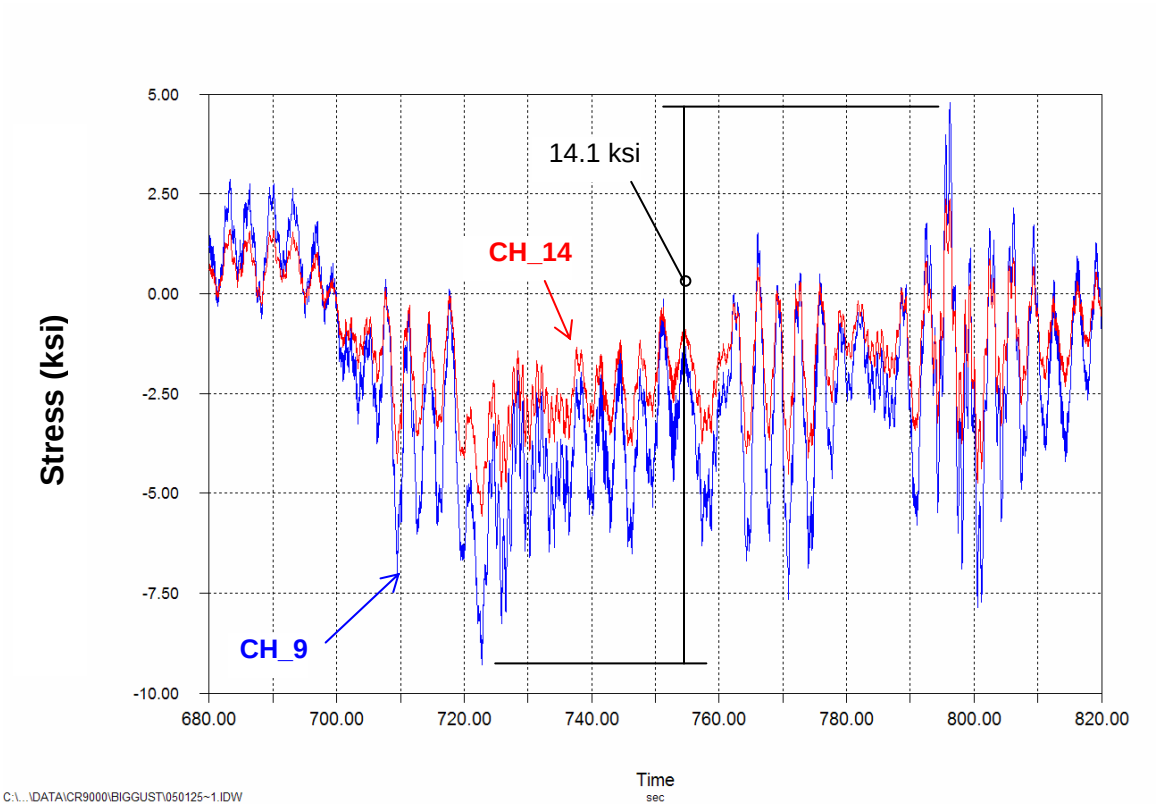

Figure 4.13– Detailed stress time-history for a large wind event
at the As-built tower on January 22, 2005 and 5:20AM

4.4 Vortex Shedding

In this section the wind phenomena of vortex shedding will be examined. Good examples of vortex shedding were recorded at the Retrofit tower. Such an example is presented in Figure 4.14. Shown in the Figure is a segment of time equal to 30 minutes recorded on October 13, 2004. Four data traces are shown in the Figure, namely wind speed at the 33 foot elevation, wind direction (corrected to represent compass directions), strain gage CH_5, and strain gage CH_6. These strain gages are located on opposite sides of the tower on the tower just above the retrofit jacket. A zoomed-in segment of data indicated by the dashed box, is shown in Figure 4.15.

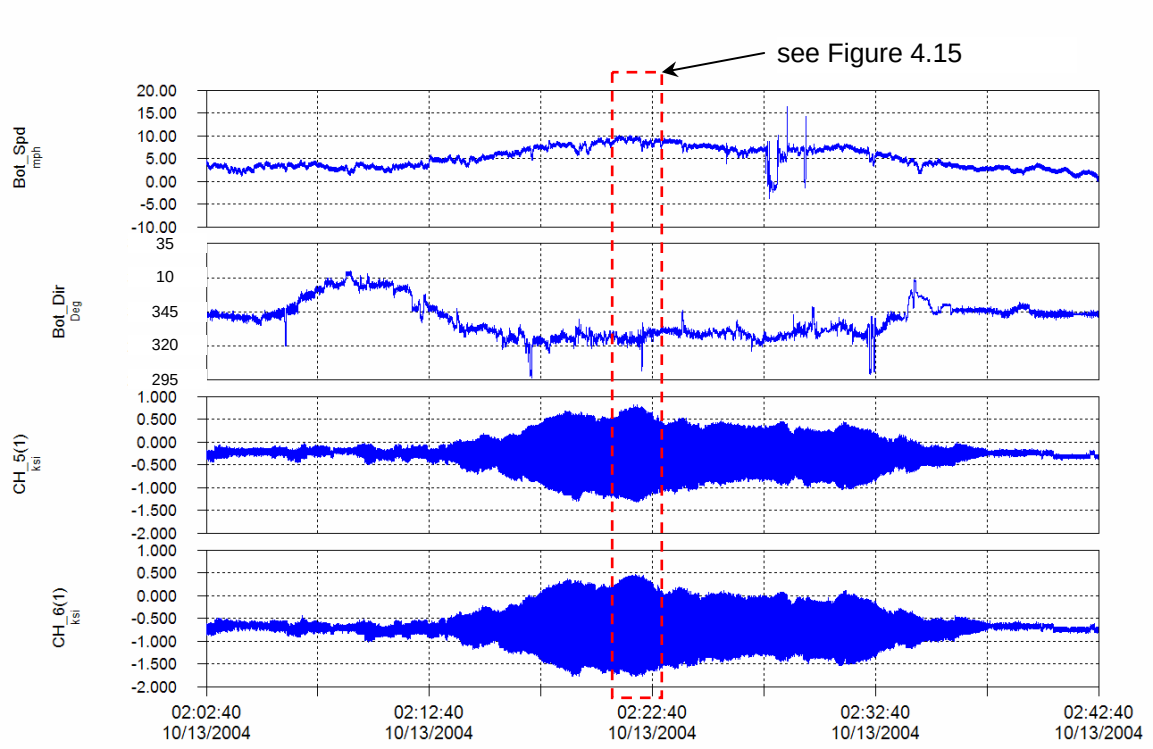

Figure 4.14 – Example of vortex shedding occurring in the second vibration mode (frequency = 1.32 Hz) showing response of strain gages CH_5 and CH_6

It can be seen in Figures 4.12 and 4.13 that the wind speed at the time of this event is low, ranging between 3 and 10 mph. When the wind speed reaches a critical value (approximately 6 mph), vortex shedding commences. When the frequency of the vortex shedding matches a vibration frequency of the tower, the tower locks-in and begins to oscillate in that mode of vibration. In this case the second mode of vibration is excited (see Figure 3.4b). The frequency of vibration is 1.32 Hz. The stress range measured in these strain gages is approximately 2 ksi. After the wind speed drops below 6 mph (the critical wind speed), the vortex shedding ends.

Though this stress is not excessively high, there are approximately 1300 stress cycles caused by this single event. It has been found that the 2nd mode vortex shedding is most common at these towers, but that the measured stress range is low. However, due to the fact that the socket connection at the base has poor fatigue resistance (the CAFL

may be less than 2.3 ksi for E'), vortex shedding has the potential to cause a large number of damage-causing cycles.

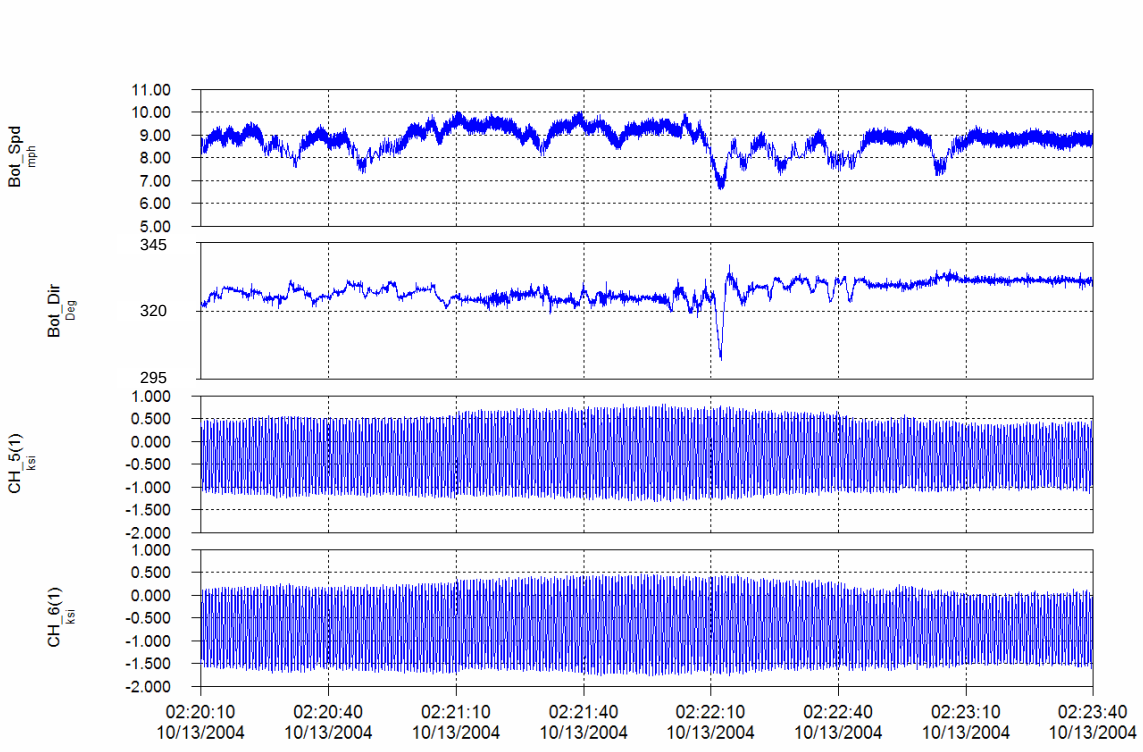

Figure 4.15 – Detail plot of vortex shedding occurring in the second vibration mode (frequency = 1.32 Hz) showing response of strain gages CH_5 and CH_6

5.0 Conclusions

Based on the results presented above, the following conclusions can be drawn:

1. Frequencies of vibration for the first four modes for all of the towers included in the testing program fall within the same range (0.25 for first mode to 7.3 Hz for the fourth mode).
2. Good agreement was observed between the measured modal frequencies and those determined through analysis.
3. In general, the measured modal damping ratios were found to be significantly lower in the higher modes of vibration.
    a. The high damping ratio in the first mode may be due to aerodynamic damping.
    b. The AASHTO and CAN/CSA specifications suggested damping ratios are significantly higher than the measured damping ratios for the higher modes. Therefore, vortex shedding response predicted by code would be unconservative.
4. As expected, the stresses in the As-built Sioux City tower are much higher than those in the Sioux City Retrofit tower.
5. Loose anchor nuts had a significant effect on the measured stresses in the tube wall of the tower adjacent to the baseplate welds.
6. Loose anchor nuts had little effect on the measured damping ratio or modal frequency.
7. Testing of a base connection with leveling nuts that were not level demonstrated that very high localized stresses are generated, and may approach the yield stress of the material in the tube wall.
8. Finite fatigue life is predicted at all locations monitored at the As-built tower in Clear Lake, with a minimum life prediction of 10 years. However, the actual fatigue life may be even less due to the uncertainty in the detail categorization (it may be even worse than E'.)
9. Effectively infinite life (over 100 years) is predicted at all locations monitored at the Retrofit tower in Clear Lake. It is suggested that additional instrumentation be installed at one of the retrofit towers to more fully verify the behavior of the jacket connection.
10. A two-lobed wind frequency distribution was measured at both the As-built and Retrofit towers in Clear Lake, with predominant winds from 160 and 315 degrees.
11. At both towers, the highest stress range cycles were caused by buffeting from natural wind gusts. Peak stresses on the order of 17.5 ksi were measured in the As-built pole (for the Retrofit pole, the peak stress was on the order of 9.4 ksi above the spice jacket).
12. Vortex shedding was observed to occur in the second vibration mode (frequency of 1.3 Hz). The measured stress ranges were lower, on the order of 2 ksi, however, there is the potential for accumulation of a large number of cycles.
13. Comparing the results of the static tests of the As-built and Retrofit towers at Sioux City, it can be seen that the stresses can be reduced significantly by increasing the baseplate thickness and tube wall of the mast. Preliminary finite element analysis of similar structures has indicated that increasing the baseplate thickness alone can reduce stresses

in the tube wall. Therefore, improved fatigue resistance can be expected simply by thickening the baseplate, which does not significantly add to the fabricated cost of a high-mast tower. A minimum baseplate thickness of 3 inches is recommended for tall (greater than 140 feet high) high-mast towers.

6.0 References

1. Dexter, R.J., *Investigation of Cracking of High-mast Lighting Towers, Iowa Department of Transportation*, Ames, IA, September 2004.
2. American Association of State Highway and Transportation Officials, *Standard Specifications for Structural Supports for Highway Signs, Luminaries and Traffic Signals, 4th Edition*, Washington, D.C., 2001.
3. CSA International, *CAN/CSA-S6-00, Canadian Highway Bridge Design Code*, Toronto, Canada, December 2000
4. CSA International, *Commentary on CAN/CSA-S6-00, Canadian Highway Bridge Design Code*, Toronto, Canada, December 2000.
5. Simiu, E., Scanlan, R.H., *Wind Effects on Structures: An Introduction on Wind Engineering*, Third Edition, John Wiley & Sons, NY, 1996.
6. Lions, R.G., *Understanding Digital Signal Processing*, Prentice Hall PTR, 2001.
7. Miner, M.A., *Cumulative Damage in Fatigue*, Journal of Applied Mechanics, Vol. 1, No.1, Sept., 1945.
8. Downing S.D., Socie D.F., *Simple Rainflow Counting Algorithms*, International Journal of Fatigue, January 1982.
9. Fisher, J.W., Nussbaumer, A., Keating, P.B., and Yen, B.T., *Resistance of Welded Details Under Variable Amplitude Long-Life Fatigue Loading, NCHRP Report 354*, National Cooperative Highway Research Program, Washington, DC, 1993.
10. *Steel Structures – Material and Design*, Draft International Standard, International Organization for Standardization, 1994.
11. Schilling, C.G., *Variable Amplitude Load Fatigue, Task A - Literature Review: Volume I - Traffic Loading and Bridge Response*, Publication No. FHWA-RD-87-059, Federal Highway Administration, Washington, DC, July 1990.
12. Moses, F., Schilling, C.G., Raju, K.S., *Fatigue Evaluation Procedures for Steel Bridges, NCHRP Report 299*, National Cooperative Highway Research Program, Washington, DC, 1987.

APPENDIX A

Instrumentation Plans

1. **As-built and Retrofit Towers – Clear Lake**
2. **As-built and Retrofit Towers – Sioux City**

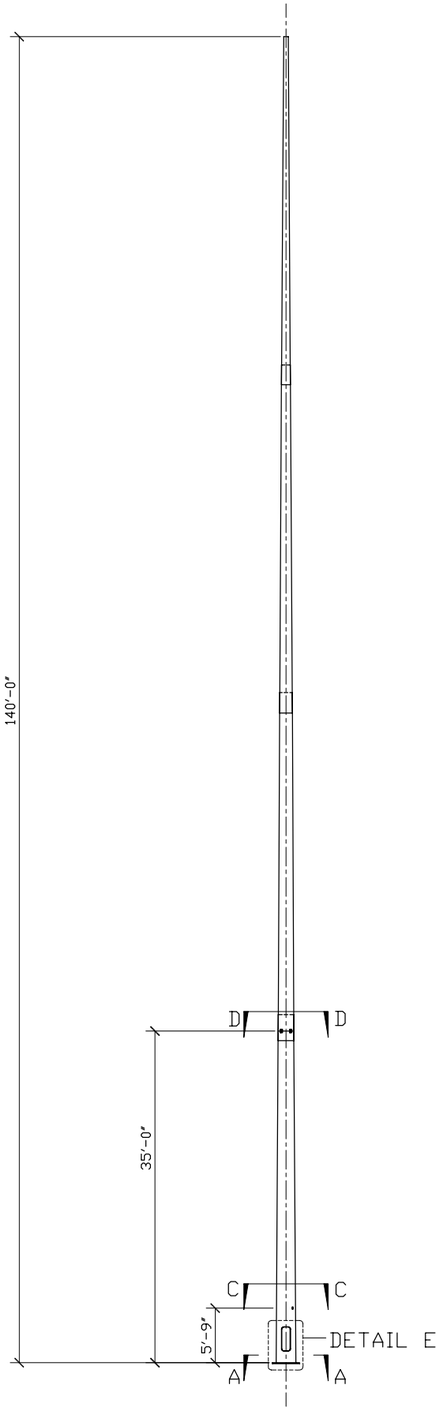

ELEVATION VIEW
SCALE: 1/16" = 1'-0"

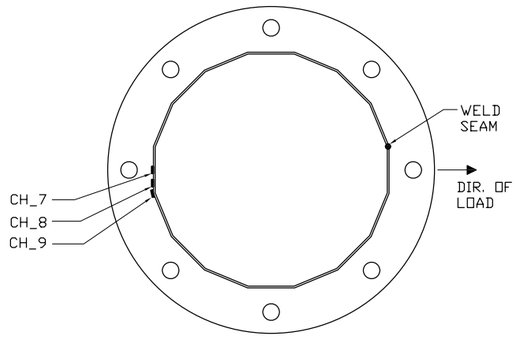

SECTION A-A
H = 0'-1 7/8"
SCALE: 3/4" = 1'-0"

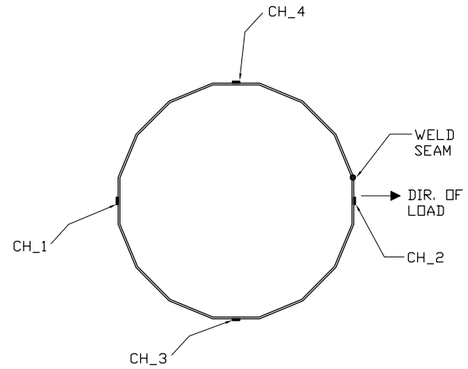

SECTION B-B
H = 0'-3"
SCALE: 3/4" = 1'-0"

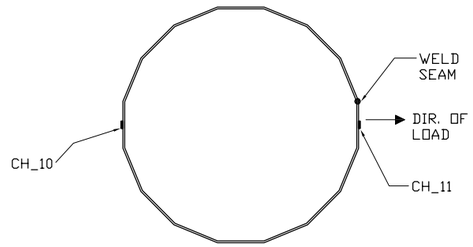

SECTION C-C
H = 0'-8"
SCALE: 3/4" = 1'-0"

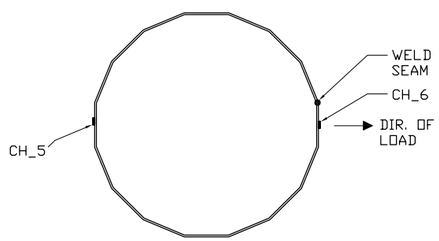

SECTION C-C
H = 5'-9"
SCALE: 3/4" = 1'-0"

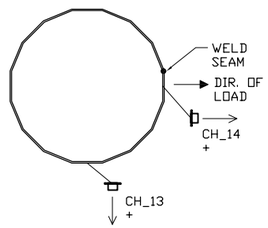

SECTION D-D
H = 35'-0"
SCALE: 3/4" = 1'-0"

LEGEND

= STRAIN GAGES (LWK-06-W250B-350)

= ACCELEROMETERS

ATLSS
ADVANCED TECHNOLOGY FOR LARGE STRUCTURAL SYSTEMS
117 ATLSS Drive
Lehigh University
Bethlehem, PA 18015
610-758-3535 FAX 610-758-6842

PROJECT:

SIOUX CITY HIGH-MAST LIGHT POLE

POLE NOTES:

AREA 1
POLE 1-B
3/4" WALL THICKNESS
2" BASE PLATE

SHEET NOTES:

1. ALL STRAIN GAGES TO BE MEASUREMENTS GROUP, INC. WELDABLE RESISTANCE GAGES TYPE LWK-06-W250B-350, U.O.N.

NO.	DESCRIPTION	DATE	BY
1	INITIAL SUBMITTAL	8/19/04	RJC

DESIGNED BY:	RJC/ICH
DRAWN BY:	ICH
CHECKED BY:	RJC
SCALE:	AS SHOWN
DATE:	8/19/04
PROJECT NO.:	
SHEET TITLE:	

INSTRUMENTATION PLAN

SHEET NO.:

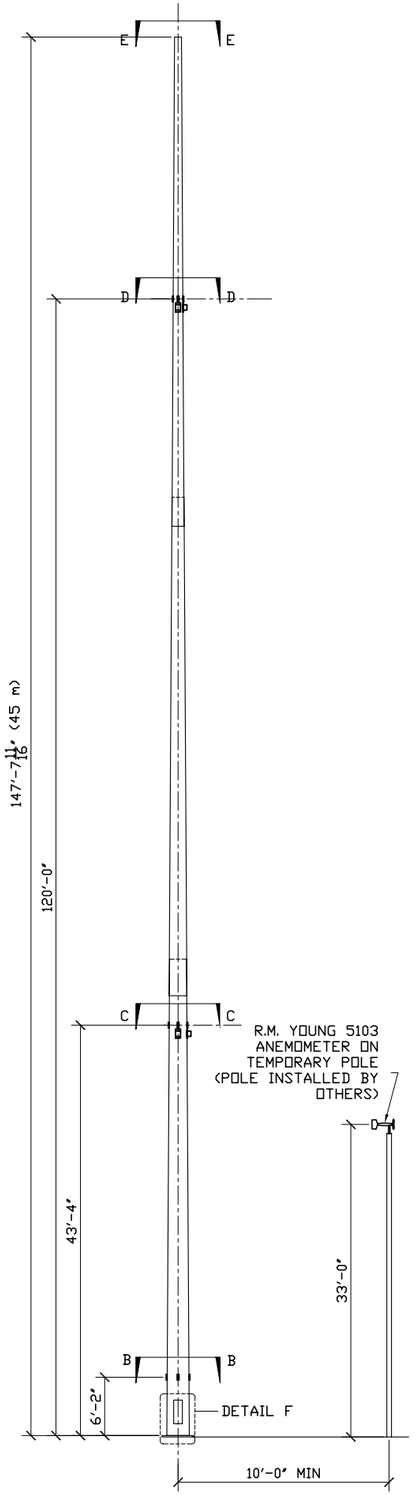

ELEVATION VIEW
SCALE: 1/16" = 1'-0"

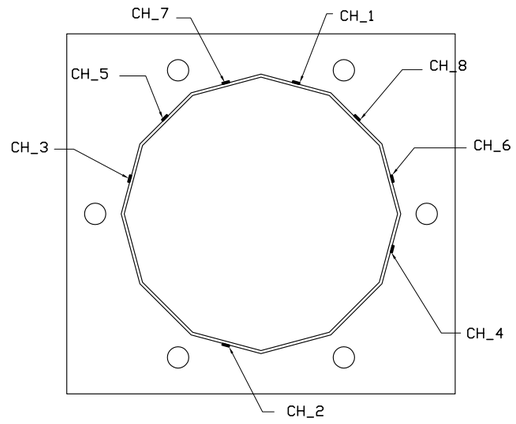

SECTION A-A
H = 0'-0"
SCALE: 3/4" = 1'-0"

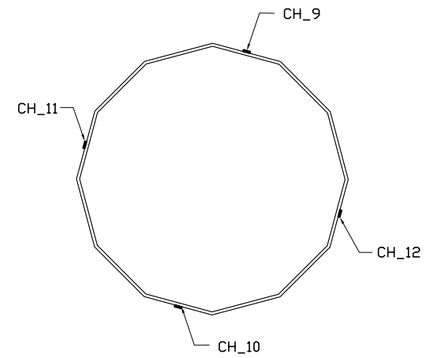

SECTION B-B
H = 5'-9"
SCALE: 3/4" = 1'-0"

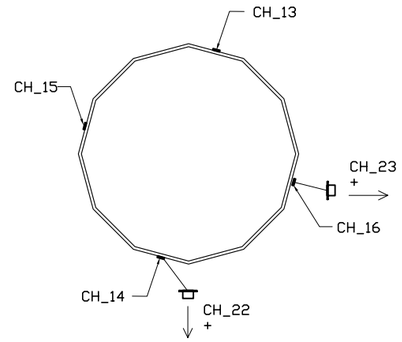

NOTE: SEE WIRING PLAN
SHEET 3 OF 3

SECTION C-C
H = 43'-4"
SCALE: 3/4" = 1'-0"

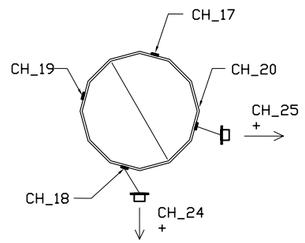

NOTE: SEE WIRING PLAN
SHEET 2 OF 2

SECTION D-D
H = 120'-0"
SCALE: 3/4" = 1'-0"

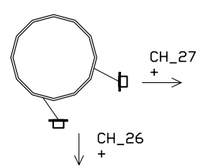

NOTE: SEE WIRING PLAN
SHEET 2 OF 2

SECTION E-E
H = 147'-7 11/16"
SCALE: 3/4" = 1'-0"

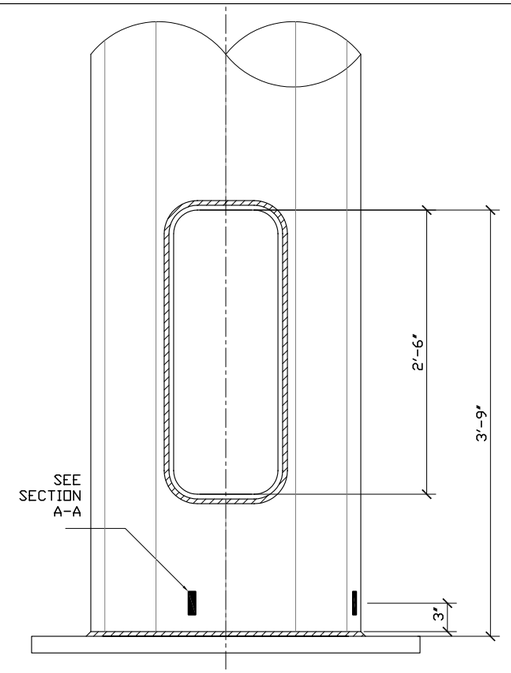

NOTE: ANCHOR BOLTS NOT SHOWN
FOR CLARITY

DETAIL F
SCALE: 3/4" = 1'-0"

ATLSS
ADVANCED TECHNOLOGY FOR
LARGE STRUCTURAL SYSTEMS
117 ATLSS Drive
Lehigh University
Bethlehem, PA 18015
610-758-3535 FAX 610-758-6842

PROJECT:

IOWA HIGH-MAST LIGHT POLE

SHEET NOTES:

1. ALL STRAIN GAGES TO BE MEASUREMENTS GROUP, INC. WELDABLE RESISTANCE GAGES TYPE LWK-06-W250B-350, U.O.N.

NO.	DESCRIPTION	DATE	BY
4	ROTATED POLE SECT.	3/31/05	ICH
3	AS-BUILT	11/17/04	ICH
2	REVISED POLE	9/13/04	RJC
1	INITIAL SUBMITTAL	8/19/04	RJC

DESIGNED BY:	RJC/ICH
DRAWN BY:	ICH
CHECKED BY:	RJC
SCALE:	AS SHOWN
DATE:	8/19/04
PROJECT NO.:	
SHEET TITLE:	

INSTRUMENTATION PLAN -PLUCK TEST

SHEET NO.:

1 OF 3

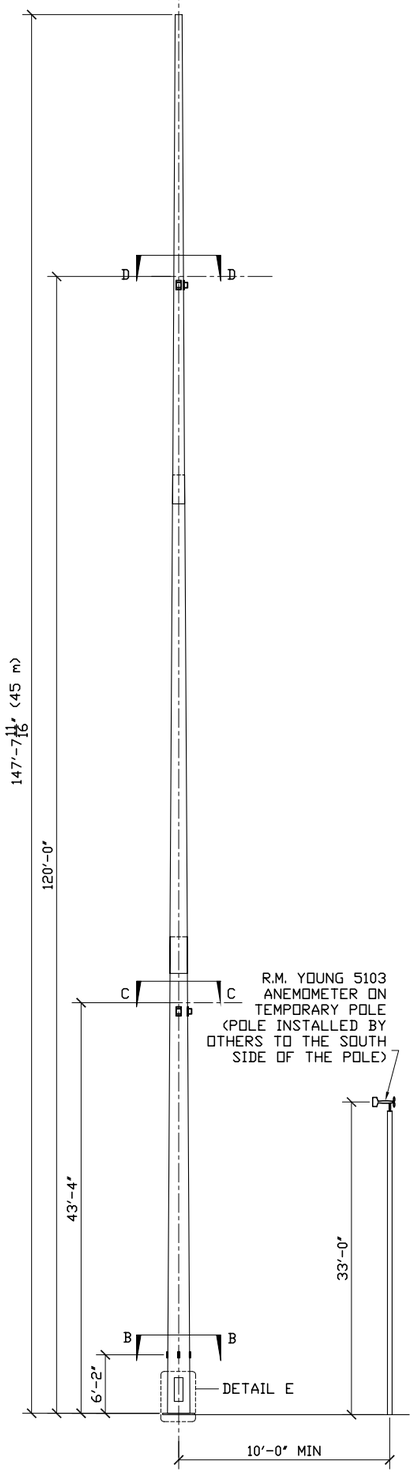

ELEVATION VIEW
SCALE: 1/16" = 1'-0"

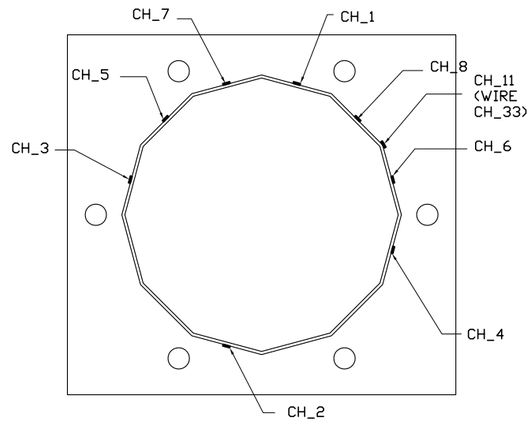

SECTION A-A
H = 0'-0"
SCALE: 3/4" = 1'-0"

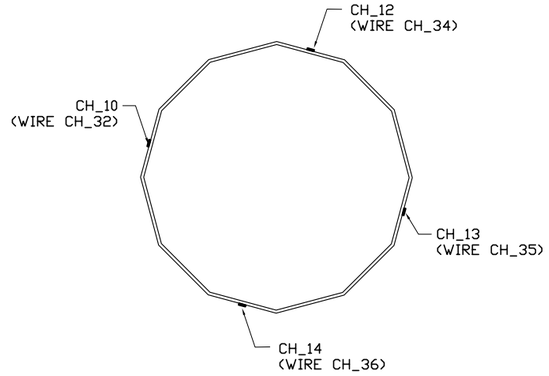

SECTION B-B
H = 5'-9"
SCALE: 3/4" = 1'-0"

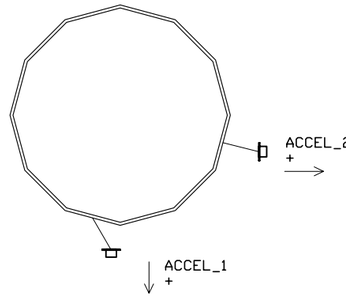

NOTE: SEE WIRING PLAN
SHEET 3 OF 3

SECTION C-C
H = 43'-4"
SCALE: 3/4" = 1'-0"

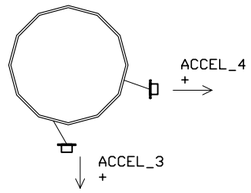

NOTE: SEE WIRING PLAN
SHEET 2 OF 2

SECTION D-D
H = 120'-0"
SCALE: 3/4" = 1'-0"

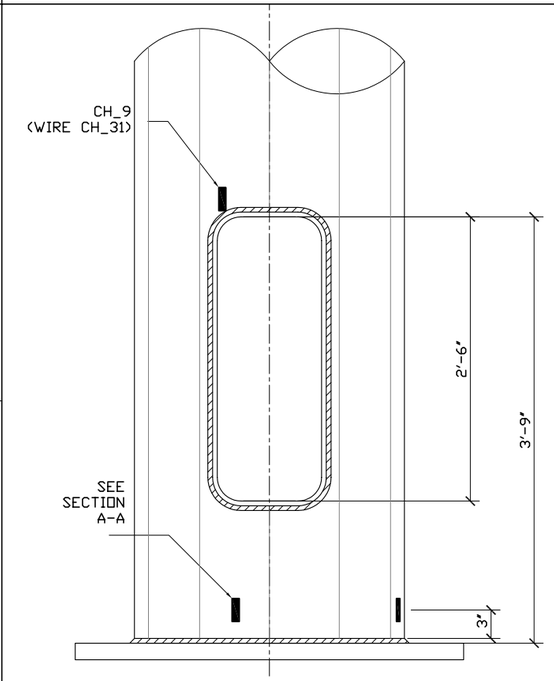

NOTE: ANCHOR BOLTS NOT SHOWN
FOR CLARITY

DETAIL E
SCALE: 3/4" = 1'-0"

ATLSS
ADVANCED TECHNOLOGY FOR
LARGE STRUCTURAL SYSTEMS
117 ATLSS Drive
Lehigh University
Bethlehem, PA 18015
610-758-3535 FAX 610-758-6842

PROJECT:

IOWA HIGH-MAST LIGHT POLE

SHEET NOTES:

1. ALL STRAIN GAGES TO BE MEASUREMENTS GROUP, INC. WELDABLE RESISTANCE GAGES TYPE LWK-06-W250B-350, U.O.N.

NO.	DESCRIPTION	DATE	BY
4	ROTATED POLE SECT.	3/31/05	ICH
3	AS-BUILT	11/17/04	ICH
2	REVISED POLE	9/13/04	RJC
1	INITIAL SUBMITTAL	8/19/04	RJC

DESIGNED BY:	RJC/ICH
DRAWN BY:	ICH
CHECKED BY:	RJC
SCALE:	AS SHOWN
DATE:	8/19/04
PROJECT NO.:	
SHEET TITLE:	

INSTRUMENTATION PLAN - LONG-TERM

SHEET NO.:

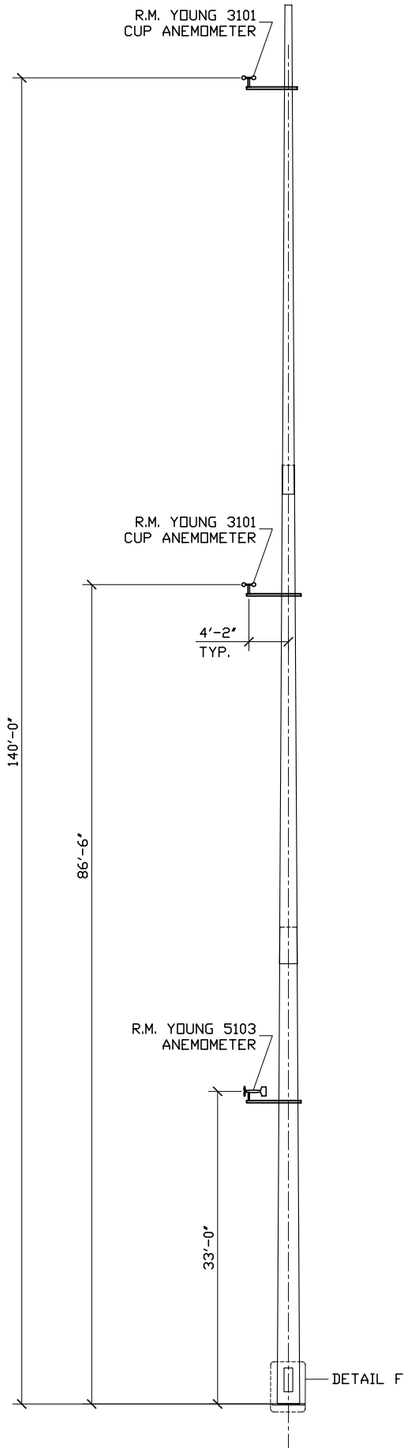

ELEVATION VIEW -
ANEMOMETER POLE
SCALE: 1/16" = 1'-0"

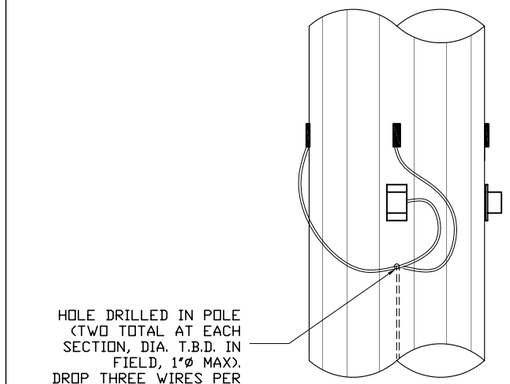

WIRING PLAN
AT SECTIONS C-C & D-D

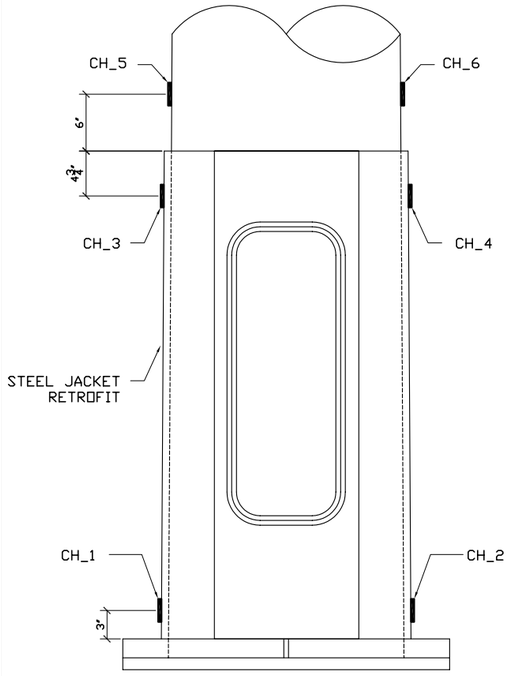

NOTE: ANCHOR BOLTS NOT SHOWN
FOR CLARITY

DETAIL F
SCALE: 3/4" = 1'-0"

ATLSS
ADVANCED TECHNOLOGY FOR
LARGE STRUCTURAL SYSTEMS
117 ATLSS Drive
Lehigh University
Bethlehem, PA 18015
610-758-3535 FAX 610-758-6842

PROJECT:

IOWA HIGH-MAST LIGHT POLE

SHEET NOTES:

1. ALL STRAIN GAGES TO BE MEASUREMENTS GROUP, INC. WELDABLE RESISTANCE GAGES TYPE LWK-06-W250B-350, U.O.N.

NO.	DESCRIPTION	DATE	BY
3	AS-BUILT	11/17/04	ICH
2	REVISED POLE	9/13/04	RJC
1	INITIAL SUBMITTAL	8/19/04	RJC

DESIGNED BY:	RJC/ICH
DRAWN BY:	ICH
CHECKED BY:	RJC
SCALE:	AS SHOWN
DATE:	8/19/04
PROJECT NO.:	
SHEET TITLE:	

INSTRUMENTATION PLAN

SHEET NO.:

3 OF 3

APPENDIX B

Development of Stress-range Histograms used to Calculate Fatigue Damage

B.1 Stress-Range Histograms

The stress-range histogram data collected during the uncontrolled monitoring permitted the development of a random variable-amplitude stress-range spectrum for the selected strain gages. It has been shown that a variable-amplitude stress-range spectrum can be represented by an equivalent constant-amplitude stress range equal to the cube root of the mean cube (rmc) of all stress ranges (i.e., Miner's rule) [7] (i.e., $S_{reff} = [\Sigma\alpha_i S_{ri}^3]^{1/3}$).

During the long-term monitoring program, stress-range histograms were developed using the rainflow cycle counting method [8]. Although several other methods have been developed to convert a random-amplitude stress-range response into a stress-range histogram, the rainflow cycle counting method is widely used and accepted for use in most structures. During the long-term monitoring program, the rainflow analysis algorithm was programmed to ignore any stress range less than 0.50 ksi (18με). Hence, the "raw" histograms do not include these very small cycles. Such small cycles do not contribute to the overall fatigue damage of even the worst details and if included, can actually unconservatively skew the results, as will be discussed below. It is also worth mentioning, that in some testing environments, the validity of stress-range cycles less than this are often questionable due to electromechanical noise.

The effective stress range presented for each channel in the body of the report was calculated by ignoring all stress-range cycles obtained from the stress-range histograms that were less than predetermined limits. (*It should be noted that the limit described here should not be confused with the limit described above. The limit above (i.e., 0.50 ksi (18με)) refers to the threshold of the smallest amplitude cycle that was counted by the algorithm and not related to the cycles that were counted, but later ignored, to ensure an accurate fatigue life estimate, as will be discussed.*) For all welded steel details, a cut-off or threshold is appropriate and necessary, as will be discussed. The limits were typically about ¼ the constant amplitude fatigue limit for the respective detail. For example, for strain gages installed at details that are characterized as category C, with a CAFL of 10.0 ksi, the cutoff was set at 2.5 ksi. Hence, stress range cycles less than 2.5 ksi were ignored in the preparation of the stress-range histograms used to calculate the effective stress range and the number of cycles accumulated. The threshold was selected for two reasons.

Previous research has demonstrated that stress ranges less than about ¼ the CAFL have little effect on the cumulative damage at the detail [9]. It has also been demonstrated that as the number of random variable cycles of lower stress range levels are considered, the predicted cumulative damage provided by the calculated effective stress range becomes asymptotic to the applicable S-N curve. A similar approach of truncating cycles of low stress range is accepted by researchers and specifications throughout the world [10].

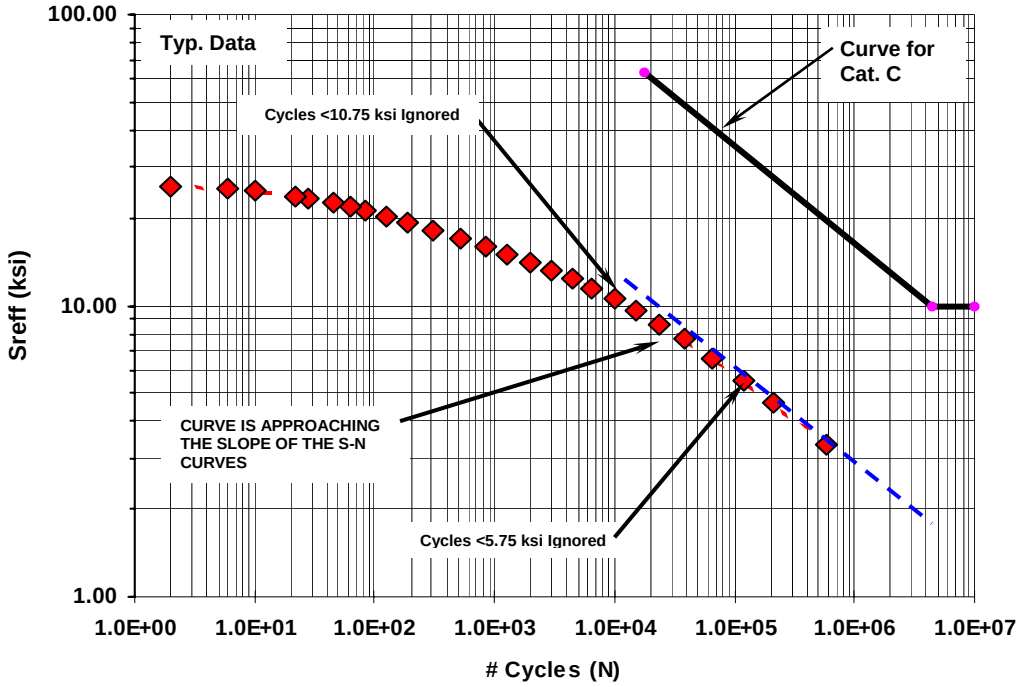

Figure B.1 – Effect of truncating cycles at different stress range cut off levels (*Typical data from a stain gage at a fatigue sensitive detail*)

Figure B.1, shows the effect on the calculated effective stress range for several levels of truncation using typical field acquired long-term monitoring data collected from strain gage installed on a bridge. The data presented in Figure B.1 are also listed in Table B.1 showing the selected truncation level and its impact on the effective stress range.

As demonstrated by Figure B.1, as the truncation level decreases (from the lowest level), the effective stress range and corresponding number of cycles approaches the slope of the S-N curve for Category C, which is also plotted in Figure B.1 (i.e., a slope of –3 on a log-log plot). As long as the cut off level selected is consistent with the slope of the fatigue resistance curve, considering additional stress cycles at lower truncation levels does not improve the damage assessment and can therefore be ignored. As can be seen, using a truncation level as high as 10 ksi, the curve is nearly asymptotic to the slope of the S-N curves. Hence, an accurate prediction of the total fatigue life results.

It should also be noted that the load spectrum assumed in the AASHTO LRFD specifications for design was developed by only considering vehicles greater than about 20 kips [11]. Thus the AASHTO LRFD design also implicitly truncates and ignores stress cycles generated by lighter vehicles and vibration [12]. The observed frequency of stress cycles obtained from traffic counts is also consistent with the frequency of vehicles measured.

Cut Off (ksi)	Number Cycles > Cut Off Value	S_{reff} (ksi)
0.75	575,867	3.3
2.75	117,869	5.5
4.75	37,842	7.6
6.75	15,112	9.6
8.75	6,547	11.5
10.75	2,938	13.3
12.75	1,284	15.1
14.75	509	17.0
16.75	191	19.3
18.75	85	21.3
20.75	45	22.6
22.75	22	23.9
24.75	6	25.1
25.75	2	25.7

Table B.1 – Calculated effective stress ranges using different stress range cut off levels
Only every other data shown in Figure B.1 is shown for brevity

The maximum stress ranges listed in the tables developed in the body of this report were determined from the rainflow count. According to rainflow cycle counting procedures, the peak and valley that comprise the maximum stress range may not be the result of a single loading event and may in fact occur hours apart. In other words, an individual truck did not *necessarily* generate the maximum stress range shown in the tables. This is particularly true of distortion induced stresses that are subjected to reversals in stress due to eccentricity of the loading. In many cases, it was possible to identify this maximum stress range with a specific vehicle passage, but in other cases, the maximum rainflow stress range exceeded the maximum stress range from any individual vehicle. During the remote long-term monitoring program, the stress-range histograms were updated every ten minutes. Hence, the longest interval between nonconsecutive peaks and valleys is ten minutes.

B.2 Frequency of Exceedence of the CAFL

Based on experimental data, it has been found that when cycles in the variable amplitude spectrum exceed the CAFL often enough, then all stress cycles experienced by the structure can be considered to be damage-causing. This frequency of exceedence limit ranges between 0.01% and 0.05%. This corresponds to an occurrence of 1 in 10,000 or 1 in 2,000.

Research indicates that if this frequency limit is not exceeded, then it is reasonable to conclude that fatigue cracking would not be expected and infinite life can be assumed. However, if the limit is exceeded, the potential for fatigue cracking of the member exists and the fatigue life can be estimated by extending the given S-N curve. Obviously, this extension will only be required if the effective stress range (S_{Reff}) is less than the CAFL of the detail.

It should be noted that the limits are somewhat different for different details and the experimental data are limited. It is perhaps overly conservative to set the limit at 0.01% one for all details when conducting a fatigue evaluation. (*This is not an issue in the design of new structures.*) However, some owners may feel that 0.05% is too liberal and that a more conservative approach is best. Therefore, for the purposes of this study, a limit of 0.01% has been used.